

Novel Sigma 1 Receptor Antagonists as Potential Therapeutics for Pain Management

Youyi Peng,* Qiang Zhang, and William J. Welsh*

Cite This: *J. Med. Chem.* 2021, 64, 890–904

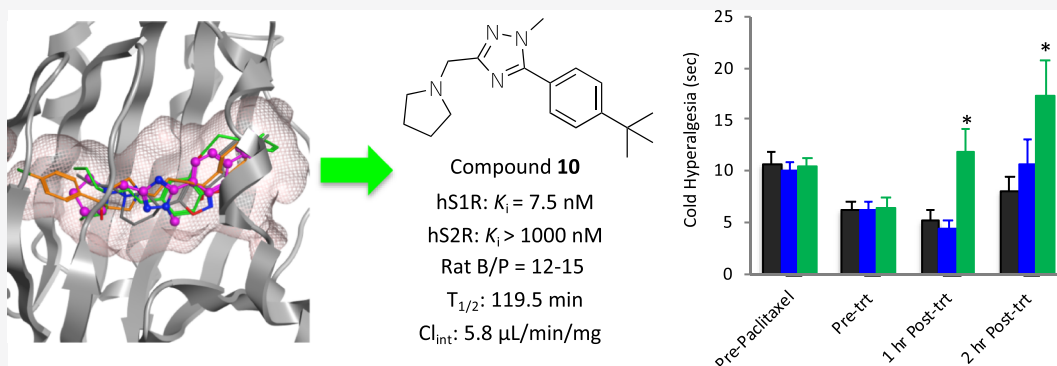
Read Online

ACCESS |

Metrics & More

Article Recommendations

Supporting Information



ABSTRACT: The sigma 1 receptor (S1R) is a molecular chaperone protein located in the endoplasmic reticulum and plasma membranes and has been shown to play important roles in various pathological disorders including pain and, as recently discovered, COVID-19. Employing structure- and QSAR-based drug design strategies, we rationally designed, synthesized, and biologically evaluated a series of novel triazole-based S1R antagonists. Compound **10** exhibited potent binding affinity for S1R, high selectivity over S2R and 87 other human targets, acceptable *in vitro* metabolic stability, slow clearance in liver microsomes, and excellent blood–brain barrier permeability in rats. Further *in vivo* studies in rats showed that **10** exhibited negligible acute toxicity in the rotarod test and statistically significant analgesic effects in the formalin test for acute inflammatory pain and paclitaxel-induced neuropathic pain models during cancer chemotherapy. These encouraging results promote further development of our triazole-based S1R antagonists as novel treatments for pain of different etiologies.

INTRODUCTION

The sigma receptor was initially identified as an opioid receptor in 1970s and later recognized as a distinct family composed of two subtypes: sigma 1 receptor (S1R) and sigma 2 receptor (S2R).^{1,2} The S1R encodes a protein of 223 amino acids in diverse species and has a molecular weight of 25.3 kDa,^{3–5} while S2R was recently identified as the protein TREM97 with 176 amino acids.⁶ The S1R is enriched in mitochondrion-associated endoplasmic reticulum (ER) membranes (MAMs)⁷ and is highly expressed in both the central and peripheral nervous systems.^{8,9}

Recent research on the S1R has implicated its role in various pathological disorders, including pain, depression, Alzheimer's disease, and Parkinson's disease.^{10–12} The S1R has been shown to act as a ligand-regulated chaperone protein and to modulate a wide spectrum of target proteins by intracellular calcium signaling.¹³ For example, it upregulates the NMDA receptor activity through the interaction with the NR1 subunit^{14,15} and modulates opioid receptors and voltage-gated calcium channels, all of which play important roles in the modulation of pain.^{16,17}

S1R knockout (KO) mice and S1R antagonists have been shown to attenuate chemical-induced (*e.g.*, formalin and capsaicin) and chemotherapy-induced neuropathic pain^{18–21} and to potentiate opioid (*e.g.* morphine and oxycodone) analgesia but not its side effects (*e.g.*, dependence, tolerance, and constipation).^{22–24} Emerging evidence also suggests that S1R antagonists may inhibit tumor growth in mouse prostate cancer xenograft models²⁵ and induce autophagic degradation of programmed death ligand 1 (PD-L1).²⁶ More recently, S1R antagonists have been found to exhibit antiviral activities against the coronavirus SARS-Cov-2 potentially *via* the interaction with the viral membrane proteins Nsp6 and Orf9c.²⁷ S1RA (MR309/E-52862, **1**, Figure 1A), a potent and selective small-molecule S1R antagonist, is the only one in

Received: November 12, 2020

Published: December 29, 2020



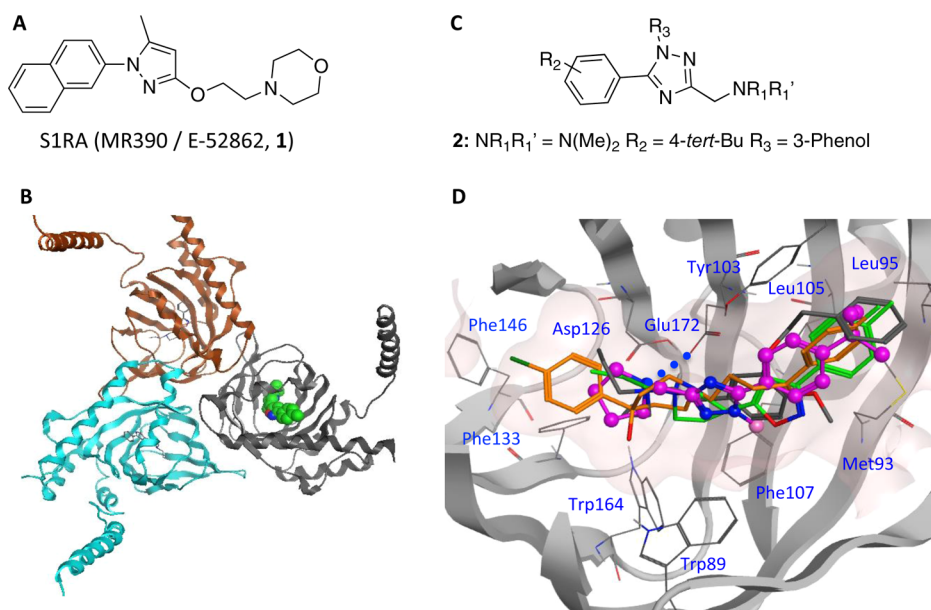


Figure 1. (A) Structure of the S1R antagonist S1RA. (B) Trimeric overall architecture of the human S1R in complex with PD144418 in the X-ray crystal structure (PDB ID: 5HK1) viewed perpendicular to the ER membrane.^{30,31} Three protomers are rendered as ribbons, and PD144418 in the A chain is rendered as a green space-filling model. (C) Structures of our novel S1R ligands with substituents R₁, R₁', R₂, and R₃: Compound **2** is (3-(5-(4-(*tert*-butyl)phenyl)-3-((dimethylamino)methyl)-1*H*-1,2,4-triazol-1-yl)phenol), with Me = methyl and Bu = butyl. (D) Superposition of our S1R ligand **10** (magenta ball-and-stick model, docked binding pose) with PD144418 (green, PDB ID: 5HK1), haloperidol (golden, PDB ID: 6DJZ), and NE-100 (dark gray, PDB ID: 6DK0) in the ligand-binding site of the human S1R crystal structure. Compound **10** was docked inside the ligand-binding pocket of the S1R crystal structure 5HK1 using GOLD.³² The salt bridge between Glu172 and the ligands is depicted as a blue dashed line. Residues engaged in extensive hydrophobic contacts with ligands are shown as solid gray lines and labeled accordingly. The topology of the ligand-binding pocket is depicted as a light-pink surface.

its kind that has advanced to phase II clinical trials. It has been shown to exhibit promising results as a treatment for chemotherapy-induced peripheral neuropathy and to potentiate opioid analgesia without inducing adverse effects such as tolerance.²⁸ However, the clinical development of S1RA has been on hold without clear reasons. We speculate that the halt was in part due to S1RA's poor oral bioavailability and/or consequent lack of sufficient efficacy, as the volunteers participating in the study were treated with very high oral doses (400 mg daily), considering its potent binding affinity for the S1R receptor ($K_i = 17$ nM).²⁹ The development of S1R antagonists with improved oral bioavailability, metabolic stability, and efficacy would represent an invaluable step forward for the management of pain without addiction and other adverse effects associated with opioid drugs.

Recently, the X-ray crystallographic structures of the human S1R in complex with several known agonists and antagonists were solved at high resolutions (2.5–3.1 Å). These crystal structures depicted a homotrimeric overall architecture with a single trans-membrane domain in each protomer (Figure 1B).^{31,33} The ligand-binding pocket of agonists and antagonists in the S1R structures was identified and revealed the detailed ligand–receptor interactions at the molecular level (Figure 1C). The availability of crystal structures of ligand-bound S1R not only helps us to understand the molecular basis for ligand recognition by the receptor but also facilitates the structure-based design of novel S1R ligands. Very recently, a structure-based virtual screening platform using these S1R crystal structures was established to successfully identify potent and selective ligands for the S1R.³⁴

During an earlier drug discovery campaign on trisubstituted 1,2,4-triazoles as potent and selective delta opioid receptor

ligands, we found that compound **2** (3-(5-(4-(*tert*-butyl)phenyl)-3-((dimethylamino)methyl)-1*H*-1,2,4-triazol-1-yl)phenol) possessed moderate affinity for the off-target sigma receptor ($IC_{50} = 560$ nM) compared with high affinity for the targeted delta opioid receptor ($IC_{50} = 5.8$ nM).³⁵ More recently, we have compiled an extensive library of diverse S1R antagonists and developed a statistically robust and highly predictive pharmacophore-based 3D-QSAR model ($R^2 = 0.92$, $Q^2 = 0.62$, $R_{pred}^2 = 0.81$).³⁰ These 3D-QSAR models, together with the availability of the ligand-bound S1R crystal structures and the promising results for S1RA in preclinical and clinical studies, motivated us to structurally optimize this series of trisubstituted 1,2,4-triazoles (Figure 1C) as high-affinity and selective S1R ligands for diverse therapeutic indications. In the present study, we report the rational design, chemical synthesis, and biological evaluation of structurally novel triazole-based S1R antagonists. The lead compound **10** exhibited potent binding affinity and high selectivity for the S1R, acceptable *in vitro* metabolic stability and clearance in liver microsomes, excellent blood–brain barrier (BBB) permeability, and *in vivo* safety and analgesic activity in rodent models.

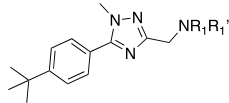
RESULTS AND DISCUSSION

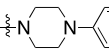
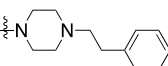
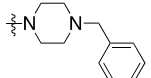
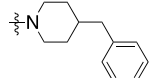
Rational Design. Starting with the high-resolution X-ray crystal structures of the human S1R in complex with several known agonists and antagonists, we proceeded to the structure-based design of novel S1R ligands. The ligand-binding pocket in the S1R structure is deeply buried and is mostly hydrophobic. The essential ligand–receptor interactions at the molecular level have been identified based on these crystal structures (Figure 1D). The anionic side chain of

Glu172 forms a salt bridge with the ligand's cationic amine, while Asp126 in its protonated state forms a hydrogen bond with Glu172 to stabilize the interaction network. Tyr103 interacts with ligands through π - π stacking and forms a hydrogen bond with Glu172 to stabilize its orientation. A number of hydrophobic residues (Trp89, Met93, Leu95, Leu105, Phe107, Phe133, Phe146, and Trp164) engage in extensive nonpolar interactions with hydrophobic or aromatic moieties of the bound ligands.

Molecular docking of compound **2** to the ligand-binding pocket of antagonist-bound S1R crystal structures (pdb ID: SHK1, 6DK0, and 6DJZ)^{31,33} indicated that the protonated basic amine atom is positioned well to form a salt bridge with the anionic side chain of Glu172. The substituents on the amine (R_1R_1' in Figure 2C and Table 1) occupy a hydrophobic subpocket surrounded by Trp89, Phe133, and Phe146. Increasing the size of R_1R_1' (dimethyl in **2**) promotes more extensive contacts with the receptor in the binding pocket. The *tert*-butylphenyl group (R_2 in Figure 2C and Table 2) is well accommodated within a hydrophobic pocket lined by several hydrophobic residues (Met93, Leu95, Leu105, and Tyr103).

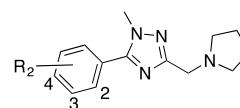
Table 1. SAR Exploration of the Basic Amine Groups^a

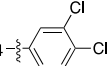


ID	-NR ₁ R ₁ '	K _i ± S.E.M. (nM)	
		S1R	S2R
(+)-Pentazocine		4.7 ± 0.11	-
Haloperidol		1.3 ± 0.26	4.7 ± 0.94
1		3.0 ± 0.62	>1000
3		3.7 ± 0.94	441 ± 78
4		56 ± 12	>1000
5		131 ± 29	>1000
6		14 ± 3.6	>1000
7		10 ± 2.1	14 ± 3.2
8		5.5 ± 1.3	39 ± 14
9		2.0 ± 0.34	57 ± 14
10		2.7 ± 0.42	474 ± 62
11		0.61 ± 0.12	324 ± 49

^aSee the Experimental Section. Assays were conducted using guinea pig whole brain homogenates. Radioligands: S1R, [³H]-(+)-pentazocine; S2R, [³H]DTG. The K_i values represent the mean ± S.E.M. of at least two independent experiments, each in duplicate.

Table 2. SAR Exploration of the Substitutions at the Phenyl Group^a



ID	R2	K _i ± S.E.M. (nM)	
		S1R	S2R
Haloperidol		2.3 ± 0.41	83 ± 14
1		24 ± 4.8	>1000
7		49 ± 7.6	17 ± 2.6
10	4- <i>tert</i> -Butyl	7.5 ± 1.7	>1000
12		9.9 ± 3.4	>1000
13	3,4-Cl ₂	22 ± 5.3	>1000
14	4-CF ₃	82 ± 21	>1000
15	3-Methyl, 4-CF ₃	21 ± 6.3	>1000
16	4-Isopropyl	96 ± 28	1000 ^c
17		26 ± 7.6	>1000
18	3- <i>tert</i> -Butyl	29 ± 7.2	1000 ^c
19		32 ± 8.9	>1000
20	4-Cl	31% ^b	>1000
21	3,4-di(Methyl)	28% ^b	>1000
22	4-Methyl	3% ^b	>1000
23	4-Cyclopropyl	30% ^b	1000 ^c
24		37% ^b	1000 ^c
25		64 ± 18	>1000
26	3-Cl,4- 	43% ^b	79% ^d
27		37 ± 9.1	1000 ^c
28	4- 	90 ± 22	60% ^d
29	3- 	40% ^b	1000 ^c
30	4- 	39% ^b	65% ^d
31	3- 	21% ^b	>1000
32	4- 	20 ± 5.4	89% ^d

^aSee the Experimental Section. Assays were conducted using human Jurkat cell homogenates. Radioligands: S1R, [³H]-(+)-pentazocine; S2R, [³H]DTG. ^bS1R binding percentage at 100 nM. ^cOne independent experimental measurement. ^dS2R binding percentage at 1000 nM. The K_i values represent the mean ± S.E.M. of at least two independent experiments, each in duplicate. Compound **10** was assayed four times in human S1R radiolabeled binding assay.

However, the phenol group on compound **2** (R_3 in Figure 2C and Table 3) is too large and clashes with the side chain of Phe107, which is consistent with its low binding affinity for the S1R. Introduction of small and hydrophobic substituents at R_3 (e.g., methyl, ethyl, isopropyl, and cyclopropyl, Table 3) helps to engage in optimal interactions with the side chain of Phe107.

Recently, we compiled a large library of diverse S1R antagonists for the development of a statistically robust and highly predictive 3D-QSAR model.³⁰ The structural motifs and their bioisosteres (e.g., *tert*-butyl vs trifluoromethylcyclopropyl) aligned at the positions of $R_1R'_1$ (Table 1) and R_2 (Table 2) on potent S1R antagonists in the diverse library were modeled onto our 1,2,4-triazole scaffold to design new ligands, all of which conformed to Lipinski's Rule of 5.³⁶ All compounds were then docked inside the ligand-binding site in the antagonist-bound S1R crystal structure (pdb ID: 5HK1) to evaluate their binding scores, followed by screening with the 3D-QSAR model to predict the S1R binding affinity (K_i). Compounds with top (high) docking scores and potent (low nM) predicted K_i values were selected for synthesis. This procedure also considered the structural diversity of the selected compounds based on our experience in drug discovery. All of the designed compounds passed the PAINS (pan assay interference compounds substructures) screening protocol.³⁷ Future X-ray crystallography studies of the S1R complexed with our lead compound are necessary to confirm the binding poses and to facilitate further optimization of the subject S1R antagonists.

Chemistry. Two synthetic routes were developed to prepare all compounds. For compounds **3–11** and **33–35** (Scheme 1), 4-*tert*-butyl benzoic acid (**I-a**) was selected as the initial starting material. Different monosubstituted hydrazines were coupled with **I-a** using pentafluorophenol (Pfp-OH) and *N*-ethyl-*N'*-(3-dimethylaminopropyl)carbodiimide hydrochloride (EDCI) as activating reagents, and the products, hydrazides **I-b**, were isolated from its isomers without any difficulty by column chromatography. The triazole rings were subsequently cyclized by reacting **I-b** with ethyl-2-aminothioacetate to give **I-c**. The ethyl ester in **I-c** was further

replaced by amines, which produced key intermediates **I-d**. Final products were prepared by reducing the amide groups in **I-d** with di-*iso*-butylaluminum hydride (DIBAL-H). Most free amines of compounds **3–11** and **33–35** were eventually converted to HCl salts during HPLC purification processes to give products with superior stability.

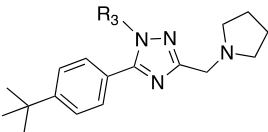
For the preparation of compounds **12–32** (Scheme 2), 1-methyl-1*H*-1,2,4-triazole-3-carboxylate (**II-a**) was used as the starting material. The 5-position of this 1*H*-1,2,4-triazole was brominated with *N*-bromosuccinimide (NBS) in moderate yields. The methyl ester group in **II-b** was converted to amide **II-d** by hydrolysis with lithium hydroxide (LiOH) and followed up by an amide coupling reaction with pyrrolidine. **II-d** was subsequently coupled with different commercially available boronic acids or internally synthesized dioxaborolanes, *via* Suzuki coupling reaction to give key intermediates **II-f**. The amide groups in **II-f** were reduced to amines with DIBAL-H to give products as free bases, which were finally converted to the corresponding HCl salts.

Compound **27** was prepared directly from compound **25**. The α position of the benzothiazepine motif in **25** was deprotonated with *n*-butyllithium (BuLi), and the resulting anion was subsequently chlorinated with NCS under mild conditions to yield compound **27** in a single step.

Structure–Activity Relationships. *In vitro* binding affinities of all compounds for the S1R and S2R were determined by radiolabeled binding assays according to previously reported methods.^{38,39} Compounds **3–11** were tested in guinea pig (g.p.) whole brain homogenates, while the other compounds were tested in human Jurkat cells using [³H]-(+)-pentazocine and [³H]DTG as the radioligands for S1R and S2R, respectively. Nonspecific binding for S1R was measured in the presence of 10 μ M unlabeled (+)-pentazocine (g.p.) or haloperidol (human). Because a selective S2R radioligand is not available, the nonselective radioligand [³H]DTG was used in the presence of an excess of (+)-pentazocine to mask the S1R. The results are summarized in Tables 1–3.

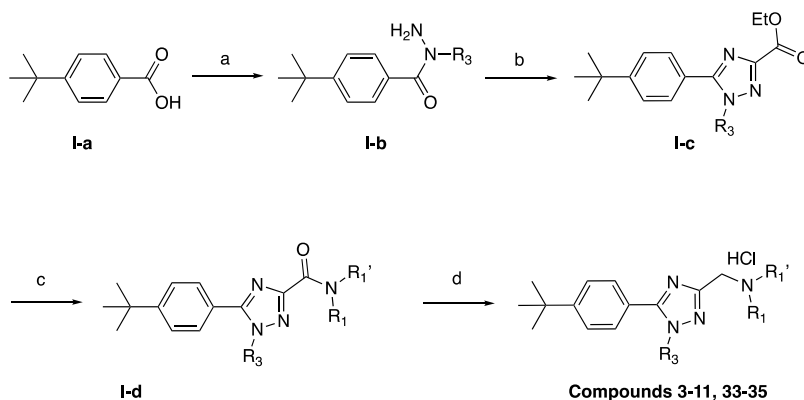
We first explored the structure–activity relationships (SARs) of the substituents ($R_1R'_1$) on the basic amine group (Table 1), guided by a combination of structure-based and QSAR-based rational design techniques. All compounds were docked inside the ligand-binding site of S1R X-ray structures using GOLD³² and the top binding pose exemplified by **10** is shown in Figure 1D. As the crystal structures and predicted binding poses reveal, the basic nitrogen atom is an essential feature to confer potent binding to the S1R, while the $R_1R'_1$ moiety sits in a hydrophobic subpocket within the ligand-binding site. Therefore, we retained the basic nitrogen atom and introduced different hydrophobic substituents to optimize ligand–receptor interactions. As the results show (Table 1), increasing the basicity of the nitrogen atom favors the binding affinity for S1R by >10 fold, as seen in piperidine-substituted **3** ($K_i = 3.7$ nM) *versus* morpholine-substituted **4** ($K_i = 56$ nM). Increasing the length of the substituent is tolerated for S1R binding affinity but enhances S2R binding affinity, as demonstrated by compounds **7** (S1R $K_i = 10$ nM, S2R $K_i = 14$ nM) *versus* **8** (S1R $K_i = 5.5$ nM, S2R $K_i = 39$ nM) *versus* **6** (S1R $K_i = 14$ nM, S2R $K_i > 1000$ nM). Introduction of a second basic nitrogen atom slightly reduces the S1R binding affinity (**9** *vs* **8**). Small pyrrolidine (**10**) and branched methylcyclopropanamine (**11**) exhibit potent binding affinities for the S1R with $K_i = 2.3$ nM

Table 3. SAR Exploration of the *N*-Substitutions on the Triazole Ring^a

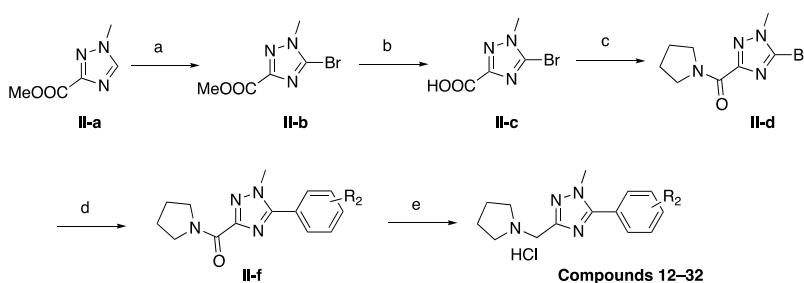


ID	R3	$K_i \pm$ S.E.M. (nM)	
		S1R	S2R
haloperidol		2.3 \pm 0.41	83 \pm 14
1		24 \pm 4.8	>1000
10	methyl	7.5 \pm 1.7	>1000
33	ethyl	4.8 \pm 0.95	1710 ^b
34	isopropyl	2.2 \pm 0.43	1460 ^b
35	cyclopropyl	14 \pm 3.8	750 ^b

^aSee the Experimental Section. Assays were conducted using human Jurkat cell homogenates. Radioligands: S1R, [³H]-(+)-pentazocine; S2R, [³H]DTG. ^bOne independent experimental measurement. The K_i values represent the mean \pm S.E.M. of at least two independent experiments, each in duplicate.

Scheme 1. Synthetic Route for Compounds 3–11 and 33–35^a

^aReagents and conditions: (a) $R_3\text{NHNH}_2$, Pfp-OH, EDCl, DIEA, DCM, 25 °C; (b) ethyl-2-amino-thioacetate, CH_3COOH , toluene, 90 °C; (c) $R_1R_1'\text{NH}$, AlMe_3 , DCE, 0–50 °C; and (d) DIBAL-H, THF, 0 °C.

Scheme 2. Synthetic Route for Compounds 12–32^a

^aReagents and conditions: (a) NaH, NBS, THF, 0–25 °C; (b) LiOH, THF, H_2O , 0–20 °C; (c) pyrrolidine, HATU, DMF, 0–20 °C; (d) $(\text{HO})_2\text{B}(\text{CH})_6R_2$ or $(\text{Me}_2\text{CHO})_2\text{B}(\text{CH})_6R_2$, K_3PO_4 , $\text{Pd}(\text{dppf})\text{Cl}_2$, 1,4-dioxane, H_2O , 20–80 °C; and (e) DIBAL-H, THF, 0 °C.

and $K_i = 0.61$ nM and high selectivity over S2R with K_i ratios of >200 and >500, respectively.

In metabolic stability studies using both human and rat liver microsomes, **10** exhibited a longer half-life and correspondingly lower clearance than **11** (Table 4). The presence of acyclic substituents at $\text{NR}_1\text{R}'_1$ of **11** would render it more labile to metabolism in liver microsomes than **10** with the more stable cyclic pyrrolidine (Table 4). Consequently, pyrrolidine at $\text{NR}_1\text{R}'_1$ of **11** was retained for the further exploration of SARs on other substitution sites (R_2 and R_3). Based on insights

Table 4. *In vitro* Metabolic Stability in Rat and Human Liver Microsomes^a

ID	rat liver microsomes		human liver microsomes	
	$T_{1/2}$ (min)	CL_{int} ($\mu\text{L}/\text{min}/\text{mg}$)	$T_{1/2}$ (min)	CL_{int} ($\mu\text{L}/\text{min}/\text{mg}$)
1	3.6	189.9	64.6	10.7
6	23.3	29.8	37.3	18.6
10	9.6	72.0	119.5	5.8
11	3.5	196.0	61.3	11.3
12	3.3	207.2	172.2	4.0
13	5.1	135.0	84.7	8.2
15	2.6	262.9	74.9	9.3
19	4.8	144.1	87.6	7.9
midazolam	2.4	292.7	2.6	262.6
diclofenac	3.5	196.2	3.7	188.8

^aSee the Experimental Section. Each test compound was incubated at 10 μM with 0.1 mg/mL rat or human liver microsomes for 1 h.

gained from our structure-based (Figure 1D) and QSAR-based virtual screening of potential S1R ligands, we introduced several hydrophobic groups at R_2 to optimize ligand–receptor binding (Table 2). These compounds were evaluated in radiolabeled binding assays using human Jurkat cells. We first compared how our compounds performed in the g.p. and human receptor binding assays. Four compounds (haloperidol, **1**, **7**, and **10**) were assayed in both assays, and their binding affinities (K_i) for both sigma receptors were found to correlate well between g.p. and human assays. Positive controls haloperidol and S1RA (**1**) exhibited binding affinities (K_i) within the literature values.^{40,41} Consequently, we felt confident that the SARs for substitutions at $\text{NR}_1\text{R}'_1$ observed in the g.p. binding assays (Table 1) should be consistent with those of the human binding assays.

As Table 2 shows, more bulky hydrophobic substituents enhanced S1R binding affinity, as seen by the descending order of receptor binding affinities (K_i): **10** (*tert*-butyl, 7.5 nM) \approx **12** (trifluoromethylcyclopropyl, 9.9 nM) > **16** (isopropyl, 96 nM) > **23** (cyclopropyl, 30% binding at 100 nM) > **22** (methyl, 3% binding at 100 nM). Substitutions at the 4-position of the phenyl ring were more favorable for S1R binding than those at the 3-position: **10** (7.5 nM) versus **18** (29.4 nM), **12** (9.9 nM) versus **19** (32 nM), **28** (90 nM) versus **29** (40% binding at 100 nM), and **30** (39% binding) versus **31** (21% binding). In general, elongation of the substituents reduced the S1R binding affinity but enhanced the S2R binding affinity, for example, **13** (S1R $K_i = 22$ nM, S2R $K_i > 1000$ nM) versus **26** (43% S1R binding at 100 nM, 79% S2R binding at 1000 nM) and **28** (S1R $K_i = 90$ nM, 60% S2R binding) versus **30** (29%

S1R binding, 65% S2R binding). Taken together, the size and hydrophobicity of the substituent at R₂ are critical features in modulating the potency (binding affinity) and selectivity for the S1R over the S2R.

Subsequent SAR studies were focused on assessing the N-substitutions (R₃) on the triazole ring by replacing methyl with three small, hydrophobic groups (ethyl, isopropyl, and cyclopropyl), keeping pyrrolidine at NR₁R₁' and 4-*tert*-butyl at R₂. Increasing the size of R₃ from methyl to isopropyl improved the S1R binding affinity by threefold but yields minimal effects on S2R (e.g., **10** vs **34**). However, introduction of a cyclopropyl (**35**, K_i = 14 nM) slightly reduced the S1R binding affinity in relation to methyl (**10**, K_i = 7.5 nM). As molecular docking shows that it is located near the side chain of Phe107 (Figure 1D), R₃ is sterically restricted. Although isopropyl is slightly larger than cyclopropyl in terms of van der Waals volume (87 Å³ vs 73 Å³, calculated with MOE), its rotational flexibility affords induced fit inside the ligand-binding pocket of S1R. Based on our molecular modeling, the rigidity of cyclopropyl raises its potential for steric clashes with the side chain of Phe107. Consequently, the isopropyl group at R₃ appears as the optimal choice for conferring potent binding affinity for S1R and high selectivity for the S1R over the S2R. However, more analogues need to be synthesized and evaluated in the binding assays to confirm this SAR.

In Vitro Metabolic Studies. Knowledge of the metabolic clearance of an absorbed drug is critical for gauging its stability, half-life, and dosing. *In vitro* metabolic stability studies were performed using rat and human liver microsomes for a subset of selected compounds to assess the effects of different substituents on liver metabolism in terms of half-life (T_{1/2}) and intrinsic clearance (CL_{int}), which are inversely proportional to each other (Table 4).

Following incubation at 10 μM with the liver microsomes for 1 h, reaction samples were analyzed by LC–MS/MS at different time points (5 min, 15 min, 30 min, and 1 h). In human liver microsomal studies, all compounds except **6** showed equivalent or superior stability (higher T_{1/2}) and lower clearance (lower CL_{int}) than the clinical candidate **1**. Compounds **10** and **12** exhibited about 2–3-fold improvement in the metabolic half-time (T_{1/2}) over **1** with T_{1/2} = 119.5 min (CL_{int} = 5.8 μL/min/mg) and T_{1/2} = 172.2 min (CL_{int} = 4.0 μL/min/mg), respectively. However, in rat liver microsomal studies, different patterns in the metabolism were observed. The majority of compounds appeared to be cleared at a similar rate as **1** except for **6** and **10**, which showed much longer half-lives (or lower intrinsic clearances) with T_{1/2} = 23.3 min (CL_{int} = 29.8 μL/min/mg) and T_{1/2} = 9.6 min (CL_{int} = 72.0 μL/min/mg), respectively. Considering the S1R binding affinity and selectivity, *in vitro* metabolic stability in liver microsomal studies, and ease of synthesis, compound **10** (S1R K_i: human 7.5 nM, g.p. 2.3 nM; S2R K_i: human >1000 nM, g.p. 474 nM; T_{1/2}: human 119.5 min, rat 9.6 min; CL_{int}: human 5.8 μL/min/mg, rat 72.0 μL/min/mg) was selected as the lead compound for further studies.

Functional Assay. We then proceeded to determine the S1R functionality of our novel ligands. Previous studies have shown that phenytoin, a low-potent allosteric modulator for the S1R, differentially modulates affinities of S1R ligands depending on their agonist versus antagonist functionality.⁴² Phenytoin potentiates the receptor binding affinity of S1R agonists (ratios of K_i without phenytoin/with phenytoin > 1); however, it produces no effects or slightly reduced receptor

binding affinity for S1R antagonists (ratios of K_i without phenytoin/with phenytoin ≤ 1). The functionality of compound **10** on S1R was determined by the radiolabeled binding assay using g.p. whole brain in the presence of phenytoin (250 μM), together with known S1R agonist dextromethorphan and antagonist haloperidol (Table 5). Both **10** and haloperidol exhibited a very small shift to lower receptor binding affinity with ratios of K_i without phenytoin/with phenytoin as 0.8 and 0.9, respectively. However, dextromethorphan showed a ratio of 6.3 in the presence of 250 μM phenytoin. These observations indicated that compound **10** acts as an antagonist for the S1R.

Selectivity Screening. To further assess its selectivity and cross-reactivity, compound **10** was tested against a diverse panel of 87 known human targets and antitargets (SafetyScreen87) at 1 μM, including GPCRs, ion channels, transporters, nuclear receptors, and enzymes. Some of the targets have been well established as contributors to clinical adverse drug reactions and should be avoided for any drugs to bind if possible.⁴³ The results, summarized in Table S1 in the Supporting Information, show that no targets exhibited ≥50% binding to **10** in the binding or enzymatic assay, indicating that **10** is relatively “clean” with respect to appreciable binding to other widely known human targets and antitargets. As expected, **10** showed negligible binding to the three opioid receptors δ, κ, and μ under the tested conditions because of the lack of an essential pharmacophore feature phenol. Notably, **10** exhibited minimal (8.4%) binding to human hERG, a target responsible for the QT-interval prolongation and whose binding should be avoided.

In Vivo Pharmacokinetic Studies. Pain modulation by S1R is primarily mediated through the central nervous system. Consequently, the drug is required to transport across the blood–brain barrier (BBB) in sufficient quantities to elicit the intended pharmacological effect. In order to assess the BBB permeability of the subject S1R ligands, compound **10** was selected for *in vivo* pharmacokinetic studies in rats at 10 mg/kg *via* i.p. administration. Brain and blood samples were collected at specific time points after drug administration (N = 3 per time point). The concentrations of compound **10** in the brain and plasma samples were determined by a LC–MS/MS method. The plasma t_{1/2} of compound **10** was found to be 0.56 h (Table 6). The ratios of brain to plasma (B/P) drug concentrations at different time points spanned from 12 to 15, which indicates good BBB permeability for compound **10**.

Rotarod Test. The rotarod test is frequently used in early stages of drug development to screen out drugs that might later cause impairments in human motor coordination. To investigate the possibility that **10** could interfere with motor coordination, the motor performance was assessed in the rotarod test after a single treatment (i.p.) at two different doses (20 mg/kg and 40 mg/kg) in Sprague Dawley (SD) rats (N = 6). Gabapentin, a first-line medication for the treatment of neuropathic pain, was used as the positive control in this test at

Table 5. Ratio of K_i Values with or without Phenytoin in the S1R Radiolabeled Binding Assays

ID	K _i (nM)	K _i (nM) + phenytoin	ratio K _i without/with phenytoin
10	2.8	3.4	0.8
haloperidol	1.3	1.4	0.9
dextromethorphan	63	10	6.3

Table 6. Pharmacokinetic Properties of Compound 10 Dosed at 10 mg/kg (i.p.) in Rats

plasma PK parameter	
$t_{1/2}$ (h)	0.56
t_{max} (h)	0.25
C_{max} (ng/mL)	932
AUC ₀₋₄ (h·ng/mL)	633
AUC _{0-inf} (h·ng/mL)	635
MRT _{inf} (h)	0.73
ratio (brain/plasma)	12–15

its equivalent therapeutic dose, 100 mg/kg (i.p.). Compound **10** did not induce any statistically significant effects on motor impairment in rats after the administration at both doses (Figure 2A). At $t = 60$ min, the motor performance was slightly reduced (without statistical significance) by **10** but quickly resumed to normal at $t = 90$ min. In contrast, gabapentin exhibited significant ($p < 0.05$) effects in reducing rats' motor coordination on the rotating rod at $t = 60$ min, 90 min, and

120 min compared to the vehicle group. These data indicate that **10** is safe in this rotarod test at both doses.

Formalin Test. The antinociceptive efficacy of compound **10** was first assessed using the rat formalin test, a widely used model in which 2% formalin solution is injected to the hind paw of the rats and biphasic pain responses are characterized by analyzing the behavior of licking the affected hind paw.^{44,45} The acute phase (0–10 min) mostly represents nociceptive pain, while the late phase (after 10 min) reflects the inflammatory responses. In this study, after rats were administered (i.p.) with compound **10** at two doses (20 mg/kg and 40 mg/kg), the time spent licking the hind paw after the injection of formalin was recorded (Figure 2B). Compared with the vehicle group, compound **10** significantly attenuated paw-licking behaviors in both phases at 40 mg/kg and only in the late phase at 20 mg/kg. In contrast, gabapentin at 100 mg/kg (i.p.) produced reduction in the paw-licking behaviors only in the late phase.

Paclitaxel-Induced Neuropathic Pain Model. Chemotherapy-induced peripheral neuropathy is one of the most serious complications associated with anticancer drugs, and its

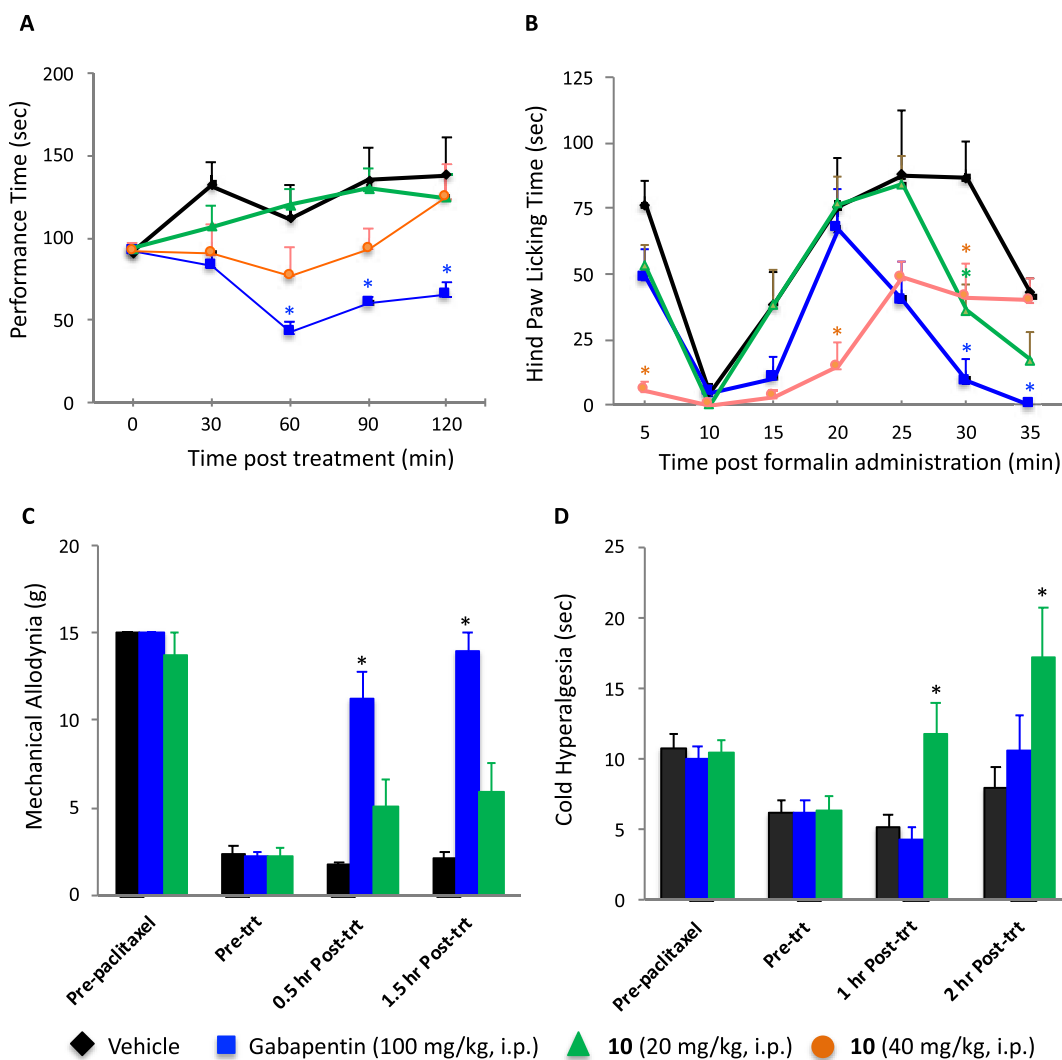


Figure 2. *In vivo* safety and efficacy studies of compound **10** in SD rats. (A) Rotarod test ($N = 6$). (B) Formalin tests ($N = 6$). (C) Mechanical allodynia in rat models of paclitaxel (Taxol)-induced neuropathic pain ($N = 8$). (D) Cold hyperalgesia in rat models of paclitaxel (Taxol)-induced neuropathic pain ($N = 8$). Pre-trt: pretreatment; Post-trt: post-treatment. In contrast, the “gold standard” drug gabapentin was used as the positive control in these studies. * p -value < 0.05 in ANOVA vs the vehicle. Data are expressed as mean \pm S.E.M. (error bars).

symptoms include allodynia and hyperalgesia. Paclitaxel, a commonly used anticancer chemotherapy, can cause dose-limiting painful peripheral neuropathy when given intraperitoneally (i.p.) and has been widely used preclinically to evaluate the analgesic effects of various drugs in neuropathic pain.⁴⁶ In the present study, paclitaxel (Taxol) at a total cumulative dose of 8 mg/kg was injected (i.p.) to rats to induce neuropathic pain. Mechanical allodynia and cold hyperalgesia were measured to assess the behavioral changes caused by i.p. administration of compound **10** (20 mg/kg), the vehicle (sterile water), and gabapentin (Figure 2).

Compared with the basal values on day 0 (prepaclitaxel), the mechanical allodynia thresholds were greatly reduced by paclitaxel challenge (pretreatment), suggesting successful development of neuropathic pain (Figure 2C). At both 0.5 h and 1.5 h after i.p. administration, compound **10** appeared to alleviate mechanical allodynia by increasing the pain threshold by 180–190% compared with the vehicle. Although the alleviation of pain was tangible, it did not achieve statistical significance with $p = 0.6$ and $p = 0.1$ (ANOVA). On the other hand, gabapentin (100 mg/kg) significantly attenuated the mechanical pain at both time points in this neuropathic pain model.

Likewise, the pretreatment values of cold hyperalgesia thresholds were measured as the paw withdrawal latencies in seconds were markedly reduced after the paclitaxel challenge when compared with the basal values on day 0 (prepaclitaxel). After treatment, **10** significantly attenuated cold hyperalgesia by increasing the withdrawal latencies by 120–130% at 1 h and 2 h postdosing compared with the vehicle control (Figure 2D). Interestingly, **10** seemingly elevated the cold hyperalgesia thresholds when compared with the basal values before the paclitaxel challenge on day 0 (prepaclitaxel). However, the differences are not statistically significant at either time point with $p = 0.61$ ($t = 1$ h) and $p = 0.08$ ($t = 2$ h). On the other hand, gabapentin failed to achieve statistical significance in alleviating cold hyperalgesia in this study at both time points. It is a common observation in the same pain study of compounds with different mechanisms of action that gabapentin does show significant efficacy in attenuating mechanical allodynia but not cold hyperalgesia (Eurofins Pharmacology Discovery Services Taiwan, private communication, November 4, 2020). This may result from the heterogeneous nature of neuropathic pain and also from the suboptimal treatment plan for this study. Previously, gabapentin has been reported to elicit delayed onset of analgesic efficacy in some neuropathic pain studies after a single dose.^{47,48} The study may require extended durations to observe the significant attenuation of cold hyperalgesia in this paclitaxel-induced neuropathic pain model. Future studies with optimized treatment regimens are necessary to further assess the analgesic efficacy of compound **10** for neuropathic pain of different etiologies.

CONCLUSIONS

Employing structure- and QSAR-based design strategies, we rationally designed, chemically synthesized, and biologically evaluated a series of novel triazole-based S1R antagonists. Compound **10** exhibited potent binding affinity (S1R K_i : human 7.5 nM, g.p. 2.3 nM) and high selectivity for S1R over S2R and other 87 human targets, acceptable *in vitro* metabolic stability and intrinsic clearance in liver microsomes ($T_{1/2}$: human 119.5 min, rat 9.6 min; Cl_{int} : human 5.8 $\mu\text{L}/\text{min}/\text{mg}$, rat 72.0 $\mu\text{L}/\text{min}/\text{mg}$), and excellent BBB permeability in rats

(B/P = 12–15). Compound **10** demonstrated negligible acute toxicity in the rat rotarod test at doses up to 40 mg/kg and statistically significant analgesic effects in the rat formalin test for acute inflammatory pain and paclitaxel-induced neuropathic pain model during cancer chemotherapy. Compared with the clinical candidate **1** (S1RA), our lead compound **10** exhibited more potent S1R binding affinity and superior *in vitro* metabolic stability. The encouraging results from these proof-of-concept studies promote further development of our triazole-based S1R antagonists as novel treatments for pain of different etiologies. More studies are currently underway to assess **10** in streptozotocin-induced diabetic and nerve injury neuropathic pain models using the clinical candidate **1** as the positive control and to further optimize S1R binding affinity and drug properties.

EXPERIMENTAL SECTION

Molecular Modeling. All computational molecular modeling and docking studies were performed on an Intel Xeon CPU E5-2643 3.4 GHz processor with a memory of 64 GB RAM using Molecular Operating Environment (MOE 2018.08, Chemical Computing Group, Montreal, QC, Canada), or GOLD (version 5.7.3) from the Cambridge Crystallographic Data Centre (CCDC, Cambridge, UK).³² The binding site was defined as the atoms within 10 Å radius around the centroids of the cocrystallized ligands. GoldScore was selected as the scoring and ranking function for all docking. Binding poses were exported to MOE for analyses.

Ligands were constructed with the Builder module in MOE, and the structures were geometry optimized by energy minimization with the MMFF94X force field and partial atomic charges. All X-ray crystallographic structures (pdb ID: SHK1, 6DK0, and 6DJZ) were downloaded from the PDB (www.rcsb.org) and processed in MOE using the Structure Preparation and Protonate 3D modules with default settings. All water molecules in the crystal structures were removed prior to the calculations. Default settings were used unless specifically stated.

Chemistry. All starting materials, reagents, and solvents were purchased from commercial suppliers and used without any further purification. All reactions involving air- or moisture-sensitive reagents were performed under an argon and dry atmosphere. The progress of reactions was monitored by TLC on SiO_2 , which was coated with a fluorescence indicator. Spots were visualized by fluorescence quenching under a UV lamp. All products, unless otherwise specified, were purified by column chromatography and/or preparative reverse-phase HPLC. Column chromatography separation was performed using the Agela purification system. SiO_2 for column chromatography was amorphous, with a particle size of 40–60 μm and a pore size of 60 Å. Separation was performed with a Gilson preparative HPLC system, which was equipped with a 333/334 pump, a UV/VIS-156 detector, and a GX-281 fraction collector. The following methods were used for general compound purification: a Phenomenex Luna C18 150 \times 30 mm column with a particle size of 5 μm was used; mobile phase A, 0.04% HCl or 0.1% TFA in water; mobile phase B, acetonitrile; the gradient was 5%–40% B in A; HPLC run time was 16 min at room temperature; flow rate was 60 mL/min; detection wavelength was 220 nm; and the gradient was optimized based on the compound polarity. ^1H and ^{13}C NMR spectra were recorded on a Bruker spectrometer with a frequency of 400 MHz and 101 MHz, respectively. Chemical shifts are reported in delta (δ) units, parts per million (ppm) downfield from tetramethylsilane (TMS). Coupling constants (J_c) are reported in hertz (Hz). Splitting patterns are designated as follows: s, singlet; br, broad singlet; d, doublet; t, triplet; q, quartet; and m, multiplet. Purity of final products (>98%) was determined by analytical HPLC at 40 °C on a Shimadzu 20AB system: a Kintex C18 2.1 \times 50 mm or a Luna C18 2.0 \times 50 mm column with a particle size of 5 μm was used; detection at 220 nm, 215 nm or 254 nm on a SPD-M20A variable wavelength detector; flow rate = 0.5 mL/min; mobile phase A, 0.037% TFA (v/v) in water;

mobile B, 0.018% TFA (v/v) in acetonitrile; gradient, 90/10–20/80 A/B in 4.5 min. The gradient was optimized based on the compound polarity. Mass spectra were recorded on a LCMS2010EV mass spectrometer from Shimadzu with electron spray ionization (ESI) as the ionization method. High-resolution mass spectral (HRMS) data were determined using an LCT Premier XE mass spectrometer from Waters. All reaction yields were not optimized.

Representative synthetic procedures of 1*H*-1,2,4-triazole derivatives for compounds are shown in Tables 1 and 3 via Scheme 1.

5-(4-(*tert*-Butyl)phenyl)-1-methyl-3-(pyrrolidin-1-ylmethyl)-1*H*-1,2,4-triazole Hydrogen Chloride (10). *Step a:* 4-(*tert*-Butyl)-*N*-methyl Benzohydrazide (*I-a*; $R_3 = \text{Me}$). 4-(*tert*-butyl) benzoic acids (*I-a*) (5.0 g, 28.1 mmol, 1.0 equiv) and Pfp-OH (5.7 g, 1.1 equiv) were mixed in 100 mL of dichloromethane (DCM) at 25 °C and EDCI (5.9 g, 1.1 equiv), followed by stirring for 4 h under a N_2 atmosphere. To another reaction flask containing DCM (100 mL), methylhydrazine-oxalic acid salt (11.5 g, 3.0 equiv) and 13.9 mL *N,N*-diisopropylethylamine (DIEA, 3.0 equiv) were added at 25 °C. The activated *I-a* solution was added dropwise to the methylhydrazine solution at 25 °C while stirring. The resulting mixture was stirred for additional 1 h. TLC was used to confirm the completion of reactions. H_2O (150 mL) was then added to quench the reaction and the mixture was extracted with DCM (80 mL \times 3). The combined organic phases were dried over Na_2SO_4 , and solvents were removed to leave the crude product as an oil, which was then loaded on a silica gel column and eluted with petroleum ether/ethyl acetate (100:1–1:1) to give compound *I-b* (4.5 g, 21.8 mmol, 83.8% yield) as a colorless oil. ^1H NMR (400 MHz CDCl_3): δ 7.52–7.34 (m, 4H), 4.44 (br s, 2H), 3.51 (s, 3H), 1.34 (s, 9H).

Step b: Ethyl 5-(4-(*tert*-Butyl)phenyl)-1-methyl-1*H*-1,2,4-triazole-3-carboxylate (*I-c*; $R_3 = \text{Me}$). Compound *I-b* (7.9 g, 41.3 mmol, 1.0 equiv) was dissolved in toluene (90 mL), followed by the addition of ethyl 2-amino-2-thioxoacetate (11.0 g, 82.6 mmol, 2.0 equiv) and acetic acid (9.0 mL). The mixture was stirred at 90 °C, and TLC indicated the completion of reaction after 12 h. The reaction mixture was poured into saturated NaHCO_3 (100 mL) and extracted with ethyl acetate (50 mL \times 3). Combined organic layers were dried over Na_2SO_4 , and solvents were removed to leave the crude product as a yellow oil, which was then loaded on a silica gel column and eluted with petroleum ether/ethyl acetate (100:1–1:1) to give compound *I-c* (8.1 g, 72.3% yield) as a yellow solid. ^1H NMR: (400 MHz, $\text{DMSO}-d_6$) δ 7.70–7.55 (m, 4H), 4.34 (qd, $J = 7.1, 11.2$ Hz, 2H), 3.49 (s, 3H), 1.35–1.28 (m, 12H).

Step c: 5-(4-(*tert*-Butyl)phenyl)-1-methyl-1*H*-1,2,4-triazol-3-yl (pyrrolidin-1-yl)methanone (*I-d*; $R_1, R'_1 = \text{cyclopentyl}$, $R_3 = \text{Me}$). To a solution of pyrrolidine (260 mg, 3.65 mmol, 1.1 equiv) in 20 mL of 1,2-dichloroethane (DCE), $\text{Al}(\text{CH}_3)_3$ (2.00 M, 4.9 mL, 3.0 equiv) was added dropwise at 0 °C. The resulting mixture was allowed to warm up to room temperature (25 °C) and was stirred for 0.5 h and then cooled to 0 °C. Compound *I-c* (950 mg, 3.32 mmol, 1.0 equiv) was added to the aforementioned mixture, which was further stirred at 50 °C for 12 h. The reaction was then cooled to 0 °C and HCl (1.0 M, 100 mL) was added to quench the reaction. DCM (30 mL \times 3) was added to extract the organic layers, which were combined and dried over Na_2SO_4 . Solvents were removed, and the residue was loaded on the silica gel column and eluted with petroleum ether/ethyl acetate (100:1–0:1) to give compound *I-d* (0.50 g, 47.9% yield) as a yellow oil. ^1H NMR: (400 MHz, CDCl_3): δ 7.65 (d, $J = 8.4$ Hz, 2H), 7.53 (d, $J = 8.4$ Hz, 2H), 4.04 (s, 3H), 3.94 (t, $J = 6.4$ Hz, 2H), 3.71 (t, $J = 6.4$ Hz, 2H), 1.90–1.97 (m, 4H), 1.36 (s, 9H).

Step d: 5-(4-(*tert*-Butyl)phenyl)-1-methyl-3-(pyrrolidin-1-ylmethyl)-1*H*-1,2,4-triazole Hydrogen Chloride (10). To a solution of the compound *I-d* (8.7 g, 28.0 mmol, 1.0 equiv) in THF (80 mL), DIBAL-H (1 M, 70 mL, 2.5 equiv) was added dropwise at 0 °C. The reaction was stirred at 0 °C for 5 h. HCl (3 M, 75 mL) was added dropwise slowly to maintain temperature at <5 °C. Ethyl acetate (50 mL \times 3) was then added to extract neutral impurities. The basicity of the aqueous solution was adjusted to pH = 14 with NaOH (2 N), and the mixture was extracted with ethyl acetate (50 mL \times 2). All organic layers were washed with brine and dried over Na_2SO_4 . All

solvents were subsequently removed. HCl (4 N in ethyl acetate, 100 mL) was then added to the residue and the resulting solution was stirred at 25 °C for 3 h, which yielded white solid precipitates. The solid was filtered and washed with ethyl acetate (30 mL) to yield the crude compound 10 (6.0 g), which was dissolved in 50 mL of H_2O , followed by the addition of NaOH (2 N) to adjust the basicity to pH = 14. Ethyl acetate (100 mL) was then added to the aqueous mixture. The organic layer was separated and washed with brine and dried over Na_2SO_4 . All solvents were then removed under reduced pressure, and the crude product was purified by reversed-phase chromatography under acidic conditions. The fractions containing the product were combined and lyophilized to give compound 10 (4.8 g, 51.3% yield, purity 98.3% as an off-white solid). The total yield was 14.9%. ^1H NMR: (400 MHz, CDCl_3): δ 12.88–13.13 (br s, 1H), 7.60 (d, $J = 8.4$ Hz, 2H), 7.54 (d, $J = 8.4$ Hz, 2H), 4.33 (s, 2H), 4.01 (s, 3H), 3.15–3.82 (m, 4H), 1.75–2.51 (m, 4H), 1.36 (s, 9H). ^{13}C (101 MHz, $\text{DMSO}-d_6$): δ 155.41, 154.56, 153.52, 128.82, 126.16, 124.73, 53.47, 49.66, 37.75, 35.09, 31.38, 23.25. HRMS (ESI) m/z : for $\text{C}_{18}\text{H}_{26}\text{N}_4$ calcd $[\text{M} + \text{H}]^+$, 299.2157; found, 299.2162.

1-((5-(4-(*tert*-Butyl)phenyl)-1-methyl-1*H*-1,2,4-triazol-3-yl)-methyl)piperidine (3). This compound was obtained using the same procedure used to synthesize compound 10. Off-white solid; yield 14.5%; purity 98.2%. ^1H NMR (400 MHz, CDCl_3) δ 7.63 (d, $J = 7.2$ Hz, 2H), 7.53 (d, $J = 7.7$ Hz, 2H), 3.98 (s, 3H), 3.63 (s, 3.73 (m, 2H), 2.62 (b, 4H), 1.67 (b, 4H), 1.37 (b, 2H), 1.27 (s, 9H). MS (ESI) m/z $[\text{M} + \text{H}]^+$: calcd, 313.2; found, 313.3.

4-((5-(4-(*tert*-Butyl)phenyl)-1-methyl-1*H*-1,2,4-triazol-3-yl)-methyl)morpholine (4). This compound was obtained using the same procedure used to synthesize compound 10. Off-white solid; yield 14.4%; purity 99.1%. ^1H NMR (400 MHz, CDCl_3): δ 7.63 (d, $J = 7.2$ Hz, 2H), 7.53 (d, $J = 7.7$ Hz, 2H), 3.98 (s, 3H), 3.63 (s, 3.73 (m, 2H), 2.62 (b, 4H), 1.67 (b, 4H), 1.37 (b, 2H), 1.27 (s, 9H). MS (ESI) m/z $[\text{M} + \text{H}]^+$: calcd, 315.2; found, 315.3.

1-((5-(4-(*tert*-Butyl)phenyl)-1-methyl-1*H*-1,2,4-triazol-3-yl)-methyl)-4-methylpiperazine (5). This compound was obtained using the same procedure used to synthesize compound 10. Lightly yellow solid; yield 12.7%; purity 99.5%. ^1H NMR (400 MHz, CDCl_3): δ 7.62 (d, $J = 7.2$ Hz, 2H), 7.51 (d, $J = 7.1$ Hz, 2H), 3.97 (s, 3H), 3.63 (s, 3.73 (s, 2H), 2.58 (b, 8H), 2.34 (s, 3H), 1.37 (s, 9H). MS (ESI) m/z $[\text{M} + \text{H}]^+$: calcd, 328.2; found, 328.1.

1-((5-(4-(*tert*-Butyl)phenyl)-1-methyl-1*H*-1,2,4-triazol-3-yl)-methyl)-4-phenethylpiperazine (6). This compound was obtained using the same procedure used to synthesize compound 10. Lightly yellow solid; yield 13.4%; purity 99.1%. ^1H NMR (400 MHz, CDCl_3) ^1H NMR (400 MHz, CDCl_3): δ 7.62 (d, $J = 7.2$ Hz, 2H), 7.51 (d, $J = 7.1$ Hz, 2H), 7.25 (m, 4H), 3.98 (s, 3H), 3.73 (b, 2H), 3.27 (b, 4H), 2.81 (b, 4H), 1.26 (s, 9H). MS (ESI) m/z $[\text{M} + \text{H}]^+$: calcd, 390.3; found, 390.2.

1-((5-(4-(*tert*-Butyl)phenyl)-1-methyl-1*H*-1,2,4-triazol-3-yl)-methyl)-4-phenethylpiperazine (7). This compound was obtained using the same procedure used to synthesize compound 10. Off-white solid; yield 14.6%; purity 98.3%. ^1H NMR (400 MHz, CDCl_3): δ 7.59 (d, $J = 7.2$ Hz, 2H), 7.50 (d, $J = 7.1$ Hz, 2H), 7.29 (m, 2H), 7.20 (s, 3H), 4.13 (s, 3H), 3.93 (b, 2H), 3.12 (b, 2H), 2.66 (b, 10H), 1.27 (s, 9H). MS (ESI) m/z $[\text{M} + \text{H}]^+$: calcd, 418.3; found, 418.2.

1-Benzyl-4-((5-(4-(*tert*-butyl)phenyl)-1-methyl-1*H*-1,2,4-triazol-3-yl)methyl)piperazine (8). This compound was obtained using the same procedure used to synthesize compound 10. Lightly yellow solid; yield 14.3%; purity 98.6%. ^1H NMR (400 MHz, CDCl_3): δ 7.63 (d, $J = 7.2$ Hz, 2H), 7.53 (d, $J = 7.7$ Hz, 2H), 7.32 (m, 4H), 7.26 (s, 1H), 3.98 (s, 3H), 3.71 (s, 2H), 3.56 (m, 2H), 2.66 (b, 8H), 1.37 (s, 9H). MS (ESI) m/z $[\text{M} + \text{H}]^+$: calcd, 404.3; found, 404.4.

4-Benzyl-1-((5-(4-(*tert*-butyl)phenyl)-1-methyl-1*H*-1,2,4-triazol-3-yl)methyl)piperidine (9). This compound was obtained using the same procedure used to synthesize compound 10. Light-yellow oil; yield 13.6%; purity 98.7%. ^1H NMR (400 MHz, CDCl_3): δ 7.63 (d, $J = 7.2$ Hz, 2H), 7.60 (d, $J = 7.2$ Hz, 2H), 7.52 (m, 3H), 7.14 (m, 2H), 3.97 (s, 3H), 3.66 (s, 2H), 3.05 (m, 2H), 2.55 (d, $J = 3.5$ Hz, 2H), 2.34 (m, 2H), 1.68 (m, 2H), 1.59 (b, 1H), 1.39 (m, 2H), 1.27 (s, 9H). MS (ESI) m/z $[\text{M} + \text{H}]^+$: calcd, 403.3; found, 403.5.

1-(5-(4-(tert-Butyl)phenyl)-1-methyl-1H-1,2,4-triazol-3-yl)-N-(cyclopropylmethyl)-N-methylmethanamine (11). This compound was obtained using the same procedure used to synthesize compound 10. Light-yellow oil; yield 12.2%; purity 99.3%. ¹H NMR (400 MHz, CDCl₃): δ 7.63 (d, J = 7.2 Hz, 2H), 7.52 (d, J = 7.1 Hz, 2H), 3.97 (s, 3H), 3.82 (b, 2H), 2.49 (b, 5H), 1.37 (s, 9H), 1.04 (b, 1H), 0.55 (b, 2H), 0.19 (b, 2H). MS (ESI) *m/z* [M + H]⁺: calcd 313.2; found, 313.3.

5-(4-(tert-Butyl)phenyl)-1-ethyl-3-(pyrrolidin-1-ylmethyl)-1H-1,2,4-triazole Hydrogen Chloride (33). This compound was obtained using the same procedure used to synthesize compound 10. Colorless oil; yield 10.2%; purity 98.1%. ¹H NMR (400 MHz, DMSO-*d*₆): δ 10.97 (br s, 1H), 7.56–7.70 (m, 4H), 4.48 (d, J = 5.01 Hz, 2H), 4.27 (q, J = 7.21 Hz, 2H), 3.45–3.64 (m, 2H), 3.16–3.26 (m, 2H), 1.81–2.05 (m, 4H), 1.41 (t, J = 7.15 Hz, 3H), 1.33 (s, 9H). MS (ESI) *m/z* [M + H]⁺: calcd, 313.2; found, 313.2.

5-(4-(tert-Butyl)phenyl)-1-isopropyl-3-(pyrrolidin-1-ylmethyl)-1H-1,2,4-triazole Hydrogen Chloride (34). This compound was obtained using the same procedure used to synthesize compound 10. Colorless crystal; yield 11.3%; purity 98.2%. ¹H NMR (400 MHz, DMSO-*d*₆): δ 10.99–11.19 (m, 1H), 7.57–7.63 (m, 4H), 4.70 (quin, J = 6.56 Hz, 1H), 4.48 (d, J = 5.07 Hz, 2H), 3.55 (br dd, J = 10.25, 4.96 Hz, 2H), 3.14–3.27 (m, 2H), 1.83–2.03 (m, 4H), 1.44 (d, J = 6.39 Hz, 6H), 1.33 (s, 9H). MS (ESI) *m/z* [M + H]⁺: calcd 327.2; found, 327.2.

5-(4-(tert-Butyl)phenyl)-1-cyclopropyl-3-(pyrrolidin-1-ylmethyl)-1H-1,2,4-triazole Hydrogen Chloride (35). This compound was obtained using the same procedure used to synthesize compound 10. White powder; yield 10.5%; purity 98.6%. ¹H NMR (400 MHz, DMSO-*d*₆): δ 11.27 (br s, 1H), 7.91 (d, J = 8.4 Hz, 2H), 7.60 (d, J = 8.6 Hz, 2H), 4.42 (d, J = 4.9 Hz, 2H), 3.90–3.97 (m, 1H), 3.54 (br dd, J = 5.0, 10.3 Hz, 2H), 3.14–3.22 (m, 2H), 1.85–2.00 (m, 4H), 1.31–1.35 (m, 9H), 1.03–1.14 (m, 4H). MS (ESI) *m/z* [M + H]⁺: calcd, 325.2; found, 325.2.

Representative synthetic procedures of 1H-1,2,4-triazole derivatives for compounds are shown in Table 2 via Scheme 2.

1-Methyl-3-(pyrrolidin-1-ylmethyl)-5-(4-(1-(trifluoromethyl)cyclopropyl)phenyl)-1H-1,2,4-triazole Hydrogen Chloride (12). *Step a:* Methyl 5-Bromo-1-methyl-1H-1,2,4-triazole-3-carboxylate (**II-b**). NaH (4.3 g, 106.3 mmol, 60% purity, 3.0 equiv) was added to the solution of compound **II-a** (5.0 g, 35.4 mmol, 1.0 equiv) in THF (150 mL) at 0 °C. After stirring for 40 min at 0 °C, NBS (31.5 g, 177.1 mmol, 5.0 equiv) was added to the mixture, followed by stirring at 20 °C for 15 h. TLC showed that starting materials were all consumed. The reaction mixture was poured into saturated NH₄Cl (200 mL) and extracted with ethyl acetate (200 mL). The combined organic layers were washed with saturated NaCl (200 mL) and dried over Na₂SO₄. The crude product was loaded onto a silica gel column and eluted with petroleum ether: ethyl acetate = 10:1 to get compound **II-b** (2.5 g, 11.3 mmol, 32.1% yield) as yellow solid. ¹H NMR (400 MHz DMSO-*d*₆): δ 13.53 (s, 1H), 3.90 (s, 3H).

Step b: 5-Bromo-1-methyl-1H-1,2,4-triazole-3-carboxylic Acid (**II-c**). LiOH·H₂O (5.7 g, 136.3 mmol, 1.5 equiv) was added to a solution of compound **II-b** (20.0 g, 90.9 mmol, 1.0 equiv) in the mixture of THF (200 mL) and H₂O (40 mL) at 0 °C. The reaction was stirred for 12 h at 20 °C. TLC showed that compound **II-b** was consumed completely; the reaction mixture was filtered and THF was removed under reduced pressure. Diluted hydrochloric acid was then added to acidify the mixture to pH = 2 to produce white solid precipitates, which were filtered and washed with water (25 mL) and dried in vacuum to yield **II-c** (17.2 g, 83.5 mmol, 91.8% yield). It was used for the next step without further purification. ¹H NMR (400 MHz DMSO-*d*₆): δ 13.53 (s, 1H), 3.90 (s, 3H).

Step c: (5-Bromo-1-methyl-1H-1,2,4-triazol-3-yl) (pyrrolidin-1-yl)methanone (**II-d**). Pyrrolidine (3.8 g, 53.6 mmol, 4.5 mL, 1.3 equiv) was added to a solution of compound **II-c** (8.5 g, 41.3 mmol, 1.0 equiv) in DMF (150 mL), and the solution was cooled to 0 °C. Hexafluorophosphate azabenzotriazole tetramethyl uronium (HATU, 20.4 g, 53.6 mmol, 1.3 equiv) was added at 0 °C, followed by the addition of DIEA (10.7 g, 82.5 mmol, 14.4 mL, 2.0 equiv). The

reaction was allowed to warm up to 25 °C while stirring and was stirred for additional 12 h at room temperature. The reaction mixture was then concentrated and the residue was directly loaded on a silica gel column and eluted with petroleum ether: ethyl acetate = 5:1 to 0:1. The product was further purified by prep-HPLC (water (containing 0.1%TFA)-acetonitrile) to give Compound **II-d** as a yellow oil (12.4 g, 35.2 mmol, 42.7% yield). ¹H NMR (400 MHz DMSO-*d*₆): δ 3.89 (s, 3H), 3.66 (s, 2H), 3.45 (d, 2H), 1.84 (s, 4H).

Step d: (1-Methyl-5-(4-(1-(trifluoromethyl)cyclopropyl)phenyl)-1H-1,2,4-triazol-3-yl) (Pyrrolidin-1-yl) Methanone (**II-f**, R₂ = 4-(1-(trifluoromethyl)cyclopropyl)). A dioxaborolane coupling reagent, 4,4,5,5-tetramethyl-2-[4-[1-(trifluoromethyl)cyclopropyl]phenyl]-1,3,2-dioxaborolane, was prepared following the previously reported procedure.⁴⁹ Dioxane (9 mL) and H₂O (3 mL) were added into a reaction tube (20 mL), followed by the addition of compound **II-d** (600 mg, 2.3 mmol, 1.0 equiv) and then 4,4,5,5-tetramethyl-2-[4-[1-(trifluoromethyl)cyclopropyl]phenyl]-1,3,2-dioxaborolane (790 mg, 1.1 equiv), K₂CO₃ (380 mg, 1.2 equiv), and Pd(dppf)Cl₂ (94 mg, 0.05 equiv). The reaction tube was sealed and heated at 80 °C for 12 h. LC–MS indicated that all starting material was consumed. The reaction tube was cooled to room temperature and the reaction mixture was poured into ice water (15 mL). The crude product was extracted with ethyl acetate (20 mL + 15 mL), and the solvents were removed. The residue was loaded on a silica gel column and eluted with petroleum ether: ethyl acetate = 5:1 to 0:1 to give a crude product. Product **II-f** was further purified by prep-HPLC (column: Nano-micro Kromasil C₁₈ 100 × 30 mm, 5 μm; mobile phase: water(containing 0.1%TFA)-acetonitrile; 35%–55% B in 10 min) to give Compound **II-f** (0.3 g, 35.9% yield) as a yellow solid. ¹H NMR (400 MHz CDCl₃): δ 37.71–7.69 (m, 2H), 7.62 (d, J = 8 Hz, 2H), 4.04 (s, 3H), 3.96 (d, J = 8 Hz, 2H), 3.69 (s, 2H), 1.97–1.91 (m, 4H), 1.43 (t, J = 8 Hz, 2H), 1.08 (s, 2H).

Step e: 1-Methyl-3-(pyrrolidin-1-ylmethyl)-5-(4-(1-(trifluoromethyl)cyclopropyl)phenyl)-1H-1,2,4-triazole Hydrogen chloride (**12**). Compound **II-f** (0.1 g, 0.27 mmol, 1.0 equiv) was dissolved in THF (10 mL), and the solution was cooled to 0 °C. DIBAL-H (1 M, 0.68 mL, 2.5 equiv) was added to the solution while stirring, and the resulting mixture was stirred at 0 °C for additional 6 h. HCl (3 N, 20 mL) was added slowly to adjust the basicity to pH = 1. Ethyl acetate (20 mL) was added to extract neutral impurities, and then, the acidic aqueous solution was lyophilized to give the crude product as a yellow solid, which was further purified by prep-HPLC (column: Phenomenex Luna C₁₈ 150 × 30 mm, 5 μm; mobile phase: [water (containing 0.04% HCl)-acetonitrile]; 5%–40% B in 10 min) to yield compound **12** (8.0 mg, 83.9% yield, purity 99.6%) as a light-yellow solid. The total yield was 3.8%. ¹H NMR (400 MHz CDCl₃): δ 7.68–7.63 (m, 4H), 4.36 (s, 2H), 4.03 (s, 3H), 3.76 (d, J = 8 Hz, 2H), 3.31 (t, J = 8 Hz, 2H), 2.81 (t, J = 8 Hz, 2H), 1.91 (s, 2H), 1.44 (t, J = 8 Hz, 2H), 1.09 (s, 2H). ¹³C (101 MHz, CDCl₃): δ 153.66, 150.49, 139.67, 131.79, 128.82, 125.50 (q, J = 271.9 Hz), 123.71, 52.41, 47.27, 37.83, 27.70 (q, J = 33.5 Hz), 23.28, 9.60. HRMS (ESI) *m/z*: for C₁₈H₂₁F₃N₄ calcd [M + H]⁺, 351.1718; found, 351.1720.

5-(3,4-Dichlorophenyl)-1-methyl-3-(pyrrolidin-1-ylmethyl)-1H-1,2,4-triazole Hydrogen Chloride (13). This compound was obtained using the same procedure used to synthesize compound 12. Light-yellow solid; yield 9.2%; purity 99.6%. ¹H NMR (400 MHz CDCl₃): δ 7.82 (d, J = 8 Hz, 1H), 7.64 (d, J = 8 Hz, 1H), 7.55–7.52 (m, 1H), 4.35 (s, 2H), 4.04 (s, 3H), 3.79 (t, J = 4 Hz, 2H), 3.28–3.26 (m, 2H), 2.21 (d, J = 4 Hz, 2H), 1.93 (s, 2H). MS (ESI) *m/z* [M + H]⁺: calcd, 311.1; found, 311.2.

1-Methyl-3-(pyrrolidin-1-ylmethyl)-5-(4-(trifluoromethyl)phenyl)-1H-1,2,4-triazole Hydrogen Chloride (14). This compound was obtained using the same procedure used to synthesize compound 12. Off-white solid; yield 9.8%; purity 99.8%. ¹H NMR (400 MHz CDCl₃): 7.83 (s, 4H), 4.37 (s, 2H), 4.06 (s, 3H), 3.79 (t, J = 8 Hz, 2H), 3.30–3.28 (m, 2H), 2.22 (t, J = 4 Hz, 2H), 1.94 (t, J = 8 Hz, 2H). MS (ESI) *m/z* [M + H]⁺: calcd, 311.1; found, 311.2.

1-Methyl-5-(3-methyl-4-(trifluoromethyl)phenyl)-3-(pyrrolidin-1-ylmethyl)-1H-1,2,4-triazole Hydrogen Chloride (15). This compound was obtained using the same procedure used to

synthesize compound **12**. Light yellow solid; yield 13.2%; purity 99.3%. ¹H NMR (400 MHz CDCl₃): 7.79 (d, *J* = 8 Hz, 1H), 7.64 (s, 1H), 7.58 (t, *J* = 8 Hz, 1H), 4.36 (s, 2H), 4.04 (s, 3H), 3.30–3.27 (m, 2H), 2.21–2.19 (m, 2H), 2.59 (s, 3H), 2.21–2.19 (m, 2H), 1.95–1.91 (m, 2H). MS (ESI) *m/z* [M + H]⁺: calcd, 325.2; found, 325.1.

5-(4-*iso*-Propylphenyl)-1-methyl-3-(pyrrolidin-1-ylmethyl)-1*H*-1,2,4-triazole Hydrogen Chloride (16). This compound was obtained using the same procedure used to synthesize compound **12**. Light-yellow solid; yield 8.7%; purity 99.8%. ¹H NMR (400 MHz CDCl₃): 7.63 (d, *J* = 8 Hz, 2H), 7.42 (d, *J* = 8 Hz, 2H), 4.42 (s, 2H), 4.05 (s, 3H), 3.77 (s, 2H), 3.35 (s, 2H), 3.04–2.97 (m, 1H), 2.19 (s, 2H), 1.95 (s, 2H), 1.30 (d, *J* = 8 Hz, 6H). MS (ESI) *m/z* [M + H]⁺: calcd, 284.2; found, 285.2.

1-Methyl-3-(pyrrolidin-1-ylmethyl)-5-(5,6,7,8-tetrahydronaphthalen-2-yl)-1*H*-1,2,4-triazole Hydrogen Chloride (17). This compound was obtained using the same procedure used to synthesize compound **12**. Light-yellow solid; yield 8.3%; purity 99.3%. ¹H NMR (400 MHz CDCl₃): 7.37 (t, *J* = 8 Hz, 2H), 7.24 (t, *J* = 8 Hz, 1H), 4.37 (s, 2H), 4.01 (s, 3H), 3.75 (t, *J* = 4 Hz, 2H), 3.34 (d, *J* = 4 Hz, 2H), 2.85 (s, 4H), 2.18 (d, *J* = 4 Hz, 2H), 1.92 (s, 2H), 1.85 (s, 4H). MS (ESI) *m/z* [M + H]⁺: calcd, 297.2; found, 297.1.

5-(3-(*tert*-Butyl)phenyl)-1-methyl-3-(pyrrolidin-1-ylmethyl)-1*H*-1,2,4-triazole Hydrogen Chloride (18). This compound was obtained using the same procedure used to synthesize compound **12**. White solid; yield 7.2%; purity 99.6%. ¹H NMR (400 MHz CDCl₃): 7.66 (s, 1H), 7.59 (d, *J* = 8 Hz, 1H), 7.55–7.27 (m, 2H), 4.37 (s, 2H), 4.01 (s, 3H), 3.78–3.74 (m, 2H), 3.34 (t, *J* = 8 Hz, 2H), 2.19 (t, *J* = 8 Hz, 2H), 1.93 (t, *J* = 8 Hz, 2H), 1.38 (s, 2H). MS (ESI) *m/z* [M + H]⁺: calcd, 299.2; found, 299.3.

1-Methyl-3-(pyrrolidin-1-ylmethyl)-5-(3-(1-(trifluoromethyl)cyclopropyl)phenyl)-1*H*-1,2,4-triazole Hydrogen Chloride (19). This compound was obtained using the same procedure used to synthesize compound **12**. Light-yellow solid; yield 6.9%; purity 99.4%. ¹H NMR (400 MHz CDCl₃): 7.76 (s, 1H), 7.64 (t, *J* = 8 Hz, 2H), 7.54 (t, *J* = 8 Hz, 1H), 4.36 (s, 2H), 4.02 (s, 3H), 3.76 (s, 2H), 3.31 (t, *J* = 4 Hz, 2H), 2.20 (d, *J* = 4 Hz, 2H), 1.93 (s, 2H), 1.46 (t, *J* = 4 Hz, 2H), 1.11 (s, 2H). MS (ESI) *m/z* [M + H]⁺: calcd, 351.2; found, 351.3.

5-(4-Chlorophenyl)-1-methyl-3-(pyrrolidin-1-ylmethyl)-1*H*-1,2,4-triazole Hydrogen Chloride (20). This compound was obtained using the same procedure used to synthesize compound **12**. White solid; yield 8.8%; purity 99.1%. ¹H NMR (400 MHz CDCl₃): 7.64 (d, *J* = 8 Hz, 2H), 7.54 (d, *J* = 8 Hz, 2H), 4.36 (s, 2H), 4.02 (s, 3H), 3.79–3.75 (m, 2H), 3.31–3.27 (m, 2H), 2.21–2.18 (m, 2H), 1.94–1.90 (m, 2H). MS (ESI) *m/z* [M + H]⁺: calcd, 277.1; found, 277.1.

5-(3,4-Dimethylphenyl)-1-methyl-3-(pyrrolidin-1-ylmethyl)-1*H*-1,2,4-triazole Hydrogen Chloride (21). This compound was obtained using the same procedure used to synthesize compound **12**. Light-yellow solid; yield 8.1%; purity 99.7%. ¹H NMR (400 MHz CDCl₃): 7.49 (s, 1H), 7.41 (d, *J* = 9.2 Hz, 1H), 7.32 (d, *J* = 9.2 Hz, 1H), 4.43 (s, 2H), 4.04 (s, 3H), 3.78–3.82 (m, 2H), 3.33–3.36 (m, 2H), 2.36 (s, 6H), 1.99 (s, 2H), 1.95–1.98 (m, 3H). MS (ESI) *m/z* [M + H]⁺: calcd, 271.2; found, 271.1.

1-Methyl-3-(pyrrolidin-1-ylmethyl)-5-(*p*-tolyl)-1*H*-1,2,4-triazole Hydrogen Chloride (22). This compound was obtained using the same procedure used to synthesize compound **12**. Light-yellow solid; yield 10.1%; purity 99.2%. ¹H NMR (400 MHz CDCl₃): 7.57 (d, *J* = 8.4 Hz, 2H), 7.35 (d, *J* = 7.6 Hz, 2H), 4.36 (s, 2H), 4.01 (s, 3H), 3.74–3.76 (m, 2H), 3.31–3.35 (m, 2H), 2.45 (s, 3H), 2.16–2.20 (m, 2H), 1.91 (s, 2H). MS (ESI) *m/z* [M + H]⁺: calcd, 257.2; found, 257.1.

5-(4-Cyclopropylphenyl)-1-methyl-3-(pyrrolidin-1-ylmethyl)-1*H*-1,2,4-triazole Hydrogen Chloride (23). This compound was obtained using the same procedure used to synthesize compound **12**. White solid; yield 12.3%; purity 99.3%. ¹H NMR (400 MHz CDCl₃): 7.65 (d, *J* = 8 Hz, 2H), 7.25 (s, 2H), 4.52 (s, 2H), 4.09 (s, 3H), 3.79 (s, 2H), 3.36 (s, 2H), 2.21–2.22 (d, *J* = 8.4 Hz, 2H), 1.98–2.02 (m, 3H), 1.10–1.13 (m, 2H), 0.80–0.81 (m, 2H). MS (ESI) *m/z* [M + H]⁺: calcd, 283.2; found, 283.2.

5-(2,3-Dihydro-1*H*-inden-5-yl)-1-methyl-3-(pyrrolidin-1-ylmethyl)-1*H*-1,2,4-triazole Hydrogen Chloride (24). This compound was obtained using the same procedure used to synthesize compound **12**. Light-yellow solid; yield 10.6%; purity 99.7%. ¹H NMR (400 MHz CDCl₃): 7.56 (s, 2H), 7.39–7.46 (m, 2H), 4.44 (s, 2H), 4.05 (s, 3H), 3.76–3.78 (d, *J* = 5.2 Hz, 2H), 3.37–3.38 (d, *J* = 5.2 Hz, 2H), 2.99–3.02 (m, 4H), 2.12–2.20 (m, 4H), 1.97 (s, 2H). MS (ESI) *m/z* [M + H]⁺: calcd, 283.2; found, 283.3.

5-(Benzo[*b*]thiophen-6-yl)-1-methyl-3-(pyrrolidin-1-ylmethyl)-1*H*-1,2,4-triazole Hydrogen Chloride (25). This compound was obtained using the same procedure used to synthesize compound **12**. White solid; yield 8.6%; purity 99.5%. ¹H NMR (400 MHz CDCl₃): 8.22 (s, 1H), 7.97–7.99 (d, *J* = 8 Hz, 1H), 7.66 (t, *J* = 4 Hz, 1H), 7.44–7.45 (d, *J* = 5.6 Hz, 1H), 4.39 (s, 2H), 4.08 (s, 3H), 3.77 (s, 2H), 3.34 (s, 2H), 2.18–2.21 (d, *J* = 4.8 Hz, 2H), 1.93 (s, 2H). MS (ESI) *m/z* [M + H]⁺: calcd, 299.1; found, 299.0.

1-Methyl-3-(pyrrolidin-1-ylmethyl)-5-(2,3,4'-trichloro-[1,1'-biphenyl]-4-yl)-1*H*-1,2,4-triazole Hydrogen Chloride (26). This compound was obtained using the same procedure used to synthesize compound **12**. Light-yellow solid; yield 9.6%; purity 99.2%. ¹H NMR (400 MHz CDCl₃): 7.84 (s, 1H), 7.64–7.65 (d, *J* = 2.4 Hz, 1H), 7.55–7.57 (d, *J* = 8 Hz, 2H), 7.49–7.51 (d, *J* = 8 Hz, 1H), 7.32–7.34 (m, 1H), 4.35–4.37 (d, *J* = 9.2 Hz, 2H), 4.04–4.08 (d, *J* = 16 Hz, 3H), 3.78 (s, 2H), 3.29 (s, 2H), 2.21 (s, 2H), 1.94–1.95 (d, *J* = 5.6 Hz, 2H). MS (ESI) *m/z* [M + H]⁺: calcd, 421.1; found, 421.0.

5-(2-Chlorobenzo[*b*]thiophen-6-yl)-1-methyl-3-(pyrrolidin-1-ylmethyl)-1*H*-1,2,4-triazole Hydrogen Chloride (27). This compound was synthesized from compound **25**, as shown in Scheme 2. *n*-BuLi (2.5 M, 804 μL, 1.5 equiv) was added to a mixture of compound **25** (0.4 g, 1.3 mmol, 1.0 equiv) in THF (20 mL) at –78 °C under N₂, followed by the addition of NCS (357 mg, 2.6 mmol, 2.0 equiv). The mixture was stirred at –78 °C for 2 h and then poured into ice water (100 mL) and stirred for 10 min. The aqueous phase was extracted with ethyl acetate (50 mL × 3). The combined organic phase was washed with brine (100 mL), dried with anhydrous Na₂SO₄, filtered, and concentrated in vacuum. The residue was purified first by column chromatography (SiO₂, petroleum ether/ethyl acetate = 20:1 to 0:1) and then by prep-HPLC (column: Waters Prep OBD C₁₈ 150 × 40 mm; mobile phase: water (containing 0.05% HCl)–acetonitrile; B %: 5%–35%, 10 min) to give the desired compound (100 mg) as a white oil, which was further separated by SFC (column: DAICEL CHIRALCEL OD (250 × 30 mm); mobile phase: water (containing 0.1% NH₃)–MeOH; B %: 33%–33%, 10 min) to obtain the final product **27** as a light-yellow solid (40 mg, yield 8.9%; purity 99.3%). ¹H NMR (400 MHz, DMSO-*d*₆): δ 10.97 (br s, 1H), 8.47 (s, 1H), 7.98 (d, *J* = 8.44 Hz, 1H), 7.84 (d, *J* = 8.31 Hz, 1H), 7.67 (s, 1H), 4.49 (br d, *J* = 5.01 Hz, 2H), 4.05 (s, 3H), 3.57 (br d, *J* = 5.01 Hz, 2H), 3.22 (br d, *J* = 7.21 Hz, 2H), 1.86–2.03 (m, 4H). MS (ESI) *m/z* [M + H]⁺: calcd, 333.1; found, 333.2.

5-([1,1'-Biphenyl]-4-yl)-1-methyl-3-(pyrrolidin-1-ylmethyl)-1*H*-1,2,4-triazole Hydrogen Chloride (28). This compound was obtained using the same procedure used to synthesize compound **12**. White solid; yield 13.1%; purity 99.1%. ¹H NMR (400 MHz, DMSO-*d*₆): δ 10.98–11.08 (m, 1H), 7.88–7.94 (m, 4H), 7.77 (d, *J* = 7.3 Hz, 2H), 7.52 (t, *J* = 7.6 Hz, 2H), 7.41–7.46 (m, 1H), 4.49 (br d, *J* = 5.1 Hz, 2H), 4.05 (s, 3H), 3.54–3.61 (m, 2H), 3.18–3.26 (m, 2H), 1.88–2.04 (m, 4H). MS (ESI) *m/z* [M + H]⁺: calcd, 319.2; found, 319.2.

5-([1,1'-Biphenyl]-3-yl)-1-methyl-3-(pyrrolidin-1-ylmethyl)-1*H*-1,2,4-triazole Hydrogen Chloride (29). This compound was obtained using the same procedure used to synthesize compound **12**. White solid; yield 12.9%; purity 99.9%. ¹H NMR (400 MHz, DMSO-*d*₆): δ 11.04 (br s, 1H), 8.04 (s, 1H), 7.88 (d, *J* = 7.83 Hz, 1H), 7.66–7.82 (m, 4H), 7.51 (t, *J* = 7.16 Hz, 2H), 7.40–7.46 (m, 1H), 4.42–4.58 (m, 2H), 4.06 (s, 3H), 3.51–3.62 (m, 2H), 3.16–3.27 (m, 2H), 2.00 (br s, 2H), 1.84–1.97 (m, 2H). MS (ESI) *m/z* [M + H]⁺: calcd, 319.2; found, 319.1.

1-Methyl-5-(4-phenoxyphenyl)-3-(pyrrolidin-1-ylmethyl)-1*H*-1,2,4-triazole Hydrogen Chloride (30). This compound was obtained using the same procedure used to synthesize compound **12**.

White solid; yield 13.1%; purity 99.9%. ^1H NMR (400 MHz, DMSO- d_6): δ 11.24 (br s, 1H), 7.82 (d, J = 8.8 Hz, 2H), 7.46 (t, J = 7.8 Hz, 2H), 7.20–7.26 (m, 1H), 7.09–7.17 (m, 4H), 4.44 (br d, J = 4.9 Hz, 2H), 3.94–4.01 (m, 3H), 3.54 (br d, J = 5.3 Hz, 2H), 3.19 (br dd, J = 6.7, 10.5 Hz, 2H), 1.85–2.02 (m, 4H). MS (ESI) m/z $[\text{M} + \text{H}]^+$: calcd, 335.2; found, 335.2.

1-Methyl-5-(3-phenoxyphenyl)-3-(pyrrolidin-1-ylmethyl)-1H-1,2,4-triazole Hydrogen Chloride (31). This compound was obtained using the same procedure used to synthesize compound 12. White solid; yield 14.5%; purity 99.8%. ^1H NMR (400 MHz, DMSO- d_6): δ 11.11 (br s, 1H), 7.51–7.66 (m, 2H), 7.39–7.46 (m, 3H), 7.15–7.26 (m, 2H), 7.09 (d, J = 7.83 Hz, 2H), 4.41–4.48 (m, 2H), 3.99 (s, 3H), 3.52 (br dd, J = 4.89, 10.27 Hz, 2H), 3.11–3.23 (m, 2H), 1.82–2.02 (m, 4H). MS (ESI) m/z $[\text{M} + \text{H}]^+$: calcd, 335.2; found, 335.2.

5-(4-(Benzoyloxy)phenyl)-1-methyl-3-(pyrrolidin-1-ylmethyl)-1H-1,2,4-triazole Hydrogen Chloride (32). This compound was obtained using the same procedure used to synthesize compound 12. Colorless solid; yield 13.2%; purity 99.1%. ^1H NMR (400 MHz, DMSO- d_6): δ 11.41 (br s, 1H), 7.72 (d, J = 8.2 Hz, 2H), 7.41 (d, J = 8.2 Hz, 2H), 4.43 (br d, J = 4.4 Hz, 2H), 3.94–4.01 (m, 3H), 3.54 (br d, J = 5.1 Hz, 2H), 3.15–3.24 (m, 2H), 2.54–2.62 (m, 1H), 1.85–2.01 (m, 4H), 1.80 (br d, J = 7.7 Hz, 4H), 1.70 (br d, J = 12.3 Hz, 1H), 1.32–1.49 (m, 4H), 1.19–1.29 (m, 1H). MS (ESI) m/z $[\text{M} + \text{H}]^+$: calcd, 325.2; found, 325.3.

S1R Radiolabeled Binding Assay. Compounds 3–11 were assayed using the guinea pig (g.p.) whole brain according to the previously reported protocol.³⁸ The membrane preparation was resuspended in 50 mM Tris-HCl at pH = 7.4 using [^3H]-(+)-pentazocine as the radioligand. Following 1 h of incubation at 25 °C, the binding assay was terminated by addition of cold buffer. The mixture was then filtered through Whatman GF/B filters and washed with cold buffer. Radioactivity was measured using the TopCount NTX liquid scintillation counter (PerkinElmer, Waltham, MA). Nonspecific binding for S1R was measured in the presence of 10 μM unlabeled (+)-pentazocine. Compounds were tested at least two times in duplicate. (+)-Pentazocine was used as the positive control for this assay.

Compounds 12–35 were assayed using human Jurkat cells according to the previously reported protocol.³⁹ The membrane preparation was incubated in 50 mM Tris-HCl at pH = 8.0 for 2 h at 37 °C using [^3H]-pentazocine as the radioligand. Radioactivity was identified using the TopCount NTX liquid scintillation counter. Nonspecific binding for S1R is measured in the presence of 10 μM unlabeled haloperidol. Compounds were tested at least two times in duplicate. Haloperidol was used as the positive control for this assay.

S2R Radiolabeled Binding Assay. Compounds 3–11 were assayed using the guinea pig (g.p.) whole brain, while compounds 12–35 were assayed using human Jurkat cells according to previously reported methods.^{38,39} The membrane preparation was incubated in 50 mM Tris-HCl at pH = 7.4 for 1 h at 25 °C using [^3H]-DTG as the radioligand. Radioactivity was measured using the TopCount NTX liquid scintillation counter. Nonspecific binding for the S2R was measured in the presence of 10 μM unlabeled haloperidol. The S1R binding was masked using 1 μM (+)-pentazocine. Compounds were tested at least two times in duplicate. Haloperidol was used as the positive control for this assay.

Receptor binding data were analyzed by nonlinear regression of saturation and competition curves using GraphPad Prism 8.0 software (GraphPad Software, La Jolla, CA).

S1R Functional Assay. The functionality of our compounds on S1R was determined using the same radiolabeled binding assay for the S1R in the presence of phenytoin (250 μM), a low-potent allosteric modulator of the S1R, according to the previously established method.⁴² If the K_i ratios without phenytoin *versus* with phenytoin are >1 , the test compounds act as S1R agonists. However, if the K_i ratios without phenytoin *versus* with phenytoin are ≤ 1 , the compounds act as S1R antagonists.

Selectivity Profiling. The selectivity profile of compound 10 was assessed at 1 μM in a panel of 87 recognized human targets and

antitargets (SafetyScreen87) by Eurofins Panlabs Discovery Services according to their standard assay protocols.

Metabolic Stability. *In vitro* metabolic stability studies were performed by BioDuro, Inc. (Shanghai, China) using rat and human liver microsome fractions (BioIVT, Westbury, NY). Each test compound at 10 μM was incubated with 0.1 mg/mL liver microsomes and 5 mM NADPH in phosphate buffer (50 mM K_2HPO_4 , pH 7.4). The reactions were sampled at predetermined time points (e.g., 5 min, 15 min, 30 min, and 1 h), and the resulting samples were analyzed by LC–MS/MS with models of LC-20AD (Shimadzu, Kyoto, Japan) and AB Sciex 4500 (AB Sciex LLC, Toronto, Canada). Metabolic stability was determined by the disappearance of test compounds over time. The linear plots of the natural logarithm (Ln) of the remaining compound percentage (%) at each time point *versus* time were generated, and the slope was calculated by linear fitting of the curve. The *in vitro* metabolic half-life ($T_{1/2}$) was calculated using $(\text{Ln}2)/k$, where k is the biotransformation rate constant and corresponds to the slope of the Ln-linear plot. The microsomal intrinsic clearance (Cl_{int}) was estimated using the equation $\text{Cl}_{\text{int}} = (\text{Ln}2)/(T_{1/2})$ ($\mu\text{L}/\text{min}/\text{mg}$ protein). Compounds were tested at least two times in duplicate. Midazolam, dextromethorphan, diclofenac, omeprazole, and phenacetin were used as controls in this assay.

Pharmacokinetic Study in Rats. This study was performed by BioDuro, Inc., in accordance with the “Guide for the Care and Use of Laboratory Animals: Eighth Edition” in the Association for Assessment and Accreditation of Laboratory Animal Care (AAALAC)-accredited laboratory animal facility. Compound 10 at 10 mg/kg (in sterile water) was administered (i.p.) to SD male rats weighing around 250 g ($N = 3$ per group). Plasma samples were collected at the following time points, predose, 0.25, 0.5, 1, 2, and 4 h, while brain samples were collected at 0.5, 1, 2, and 4 h. Aliquots (50 μL) of plasma and brain homogenate samples were mixed with 5 μL of methanol and 200 μL of 50 ng/mL internal standard terfenadine in acetonitrile. After vortexed for 1 min and centrifuged at 4000 rpm for 15 min, the supernatant was diluted with water by fivefold (plasma samples) and twofold (brain samples) for the analysis by LC–MS/MS with models of LC-20AD (Shimadzu, Kyoto, Japan) and AB Sciex 4500 (AB Sciex LLC, Toronto, Canada). Parameters were calculated using the WinNonlin pharmacokinetic software package (Certara, Princeton, NJ).

In Vivo Safety and Efficacy Studies. These studies were conducted by Eurofins Pharmacology Discovery Services (Taibei, Taiwan). All aspects of the *in vivo* behavioral studies conformed to the “Guide for the Care and Use of Laboratory Animals: Eighth Edition” in the AAALAC-accredited laboratory animal facility.

Rotarod and Formalin Tests. Groups of six SD male rats each weighing around 180 g were included to study motor coordination. Rats were trained on a rod at a continuous accelerating speed from 4 to 30 rpm during a time period of 4 min at least three times before the study and then randomly assigned to different groups with a similar baseline. Vehicle (sterile water) and test articles were administered by i.p. injection. The rats were placed on the accelerating rotarod at 30, 60, 90, and 120 min post dosing, and the time (in seconds) that rats remained on the rotarod was recorded. Compound 10 (in sterile water) was dosed at 20 mg/kg and 40 mg/kg. Gabapentin at 100 mg/kg (i.p.) was used as the positive control in this test.

One day after the rotarod test, the rats were rerandomized to groups of six and treated with the vehicle (sterile water), positive control, and test articles (i.p.). After a period of 30 min, formalin (0.05 mL, 2% solution) was injected to the subplantars. The hind paw licking time was recorded during a 0–35 min period at 5 min intervals after the formalin challenge as a measure of analgesic activity of the test compound.

Paclitaxel-Induced Neuropathy Pain. A cohort of male SD rats, each weighing around 240 g, was used for this study and was housed individually under constant temperature, humidity, and a 12 h light–dark cycle. Mechanical allodynia and cold hyperalgesia were measured to assess the behavioral changes in these rats.

Mechanical allodynia was assessed by the manual von Frey test.⁵⁰ The animals were given 20–30 min to acclimatize prior to testing.

The paw was touched with a series of eight manual von Frey monofilaments with logarithmically incremental stiffness (0.4 g, 0.6 g, 1.0 g, 2.0 g, 4.0 g, 6.0 g, 8.0 g, and 15.0 g). The manual von Frey monofilament was applied perpendicularly from underneath the mesh floor to the central plantar surface with sufficient force to cause a slight buckling against the paw and held for approximately 6–8 s. A positive (*i.e.*, painful) response was noted, if the paw was sharply withdrawn. Ambulation was considered an ambiguous response, where the stimulus was reapplied. Mechanical threshold (50% threshold) was assessed using the up and down method following the procedure described previously.⁵⁰

Cold hyperalgesia was measured by placing rats in an ice water bath (0–2 °C) of 2.5 cm depth in a Plexiglas arena 32 cm × 32 cm × 27 cm. Withdrawal latency of the left paw was recorded and averaged twice as cold hyperalgesia assessment. A cutoff time of 30 s was used to ensure an adequate response window and to prevent permanent tissue damage. Longer times *versus* vehicle are indicative of the treatment's analgesic effect.

Mechanical allodynia and cold hyperalgesia were measured to get the baseline values prior to the paclitaxel (Taxol) injection on day 0 (prepaclitaxel). Paclitaxel was then injected (*i.p.*) at 2 mg/kg on days 1, 3, 5, and 7 with a total cumulative dose of 8 mg/kg to induce neuropathic pain. Mechanical allodynia and cold hyperalgesia were measured again on day 13 (pretreatment). The animals were randomized into groups of four based on pretreatment mechanical allodynia and cold hyperalgesia values on day 13. Compound 10 (20 mg/kg), the vehicle (sterile water), and gabapentin (100 mg/kg) were administered (*i.p.*) on day 14, followed by the measurements of mechanical allodynia at 0.5 h and 1.5 h post dosing and the measurements of cold hyperalgesia at 1.0 h and 2.0 h post dosing.

The paclitaxel-induced hypersensitivity to mechanical and cold stimuli lasts for at least several weeks and does not change significantly during the first week after the development of peripheral neuropathy on day 13 in rats.⁴⁶ In order to save animals and costs, rats were reused after a 1 week washout period following the first dosing. The animals were measured on day 20 again and rerandomized to groups of four based on the mechanical allodynia and cold hyperalgesia values. Then, on day 21, animals were redosed and measured for mechanical allodynia at 0.5 h and 1.5 h post dosing and for cold hyperalgesia at 1.0 h and 2.0 h post dosing. The measurements on days 13 and 20 were combined as the pretreatment values ($N = 8$). Additionally, the measurements on days 14 and 21 were combined as the post-treatment values ($N = 8$).

STATISTICAL ANALYSIS

One-way ANOVA was used to compare the vehicle control and test article groups. p value <0.05 is considered significant.

ASSOCIATED CONTENT

Supporting Information

The Supporting Information is available free of charge at <https://pubs.acs.org/doi/10.1021/acs.jmedchem.0c01964>.

Selectivity profiling of compound 10 in SafetyScreen 87; molecular formula strings (SMILES); ¹H NMR of all final compounds; ¹³C NMR and HRMS spectra of compounds 10 and 12; and purity report for compound 10 (PDF)
SMILES data (CSV)

AUTHOR INFORMATION

Corresponding Authors

Youyi Peng – Biomedical Informatics Shared Resource, Cancer Institute of New Jersey, Rutgers, The State University of New Jersey, New Brunswick, New Jersey 08903, United States; orcid.org/0000-0003-4797-995X; Email: pengyo@cinj.rutgers.edu

William J. Welsh – Biomedical Informatics Shared Resource, Cancer Institute of New Jersey and Department of Pharmacology, Robert Wood Johnson Medical School, Rutgers, The State University of New Jersey, New Brunswick, New Jersey 08903, United States; orcid.org/0000-0002-5618-2072; Email: welshwj@rwjms.rutgers.edu

Author

Qiang Zhang – Department of Pharmacology, Robert Wood Johnson Medical School, Rutgers, The State University of New Jersey, Piscataway, New Jersey 08854, United States

Complete contact information is available at:

<https://pubs.acs.org/10.1021/acs.jmedchem.0c01964>

Notes

The authors declare no competing financial interest.

ACKNOWLEDGMENTS

This research has been supported in part with a grant from the New Jersey Health Foundation, from the Rutgers TechAdvance/TechXpress fund, and from Rutgers-Cancer Institute of New Jersey Biomedical Informatics Shared Resource of the (P30CA072720-5917). We gratefully acknowledge access to the high-performance Computing facilities and support of the computational STEM at the Rutgers Office of Advanced Research Computing (OARC, URL: <http://oarc.rutgers.edu>).

ABBREVIATIONS USED

AAALAC, Assessment and Accreditation of Laboratory Animal Care; BBB, blood–brain barrier; BuLi, *n*-butyllithium; DCE, 1,2-dichloroethane; DCM, dichloromethane; N, *N*-diisopropylethylamine; DIBAL-H, di-*iso*-butylaluminum hydride; DMF, dimethylformamide; ER, endoplasmic reticulum; EDCI, *N*-ethyl-*N'*-(3-dimethylaminopropyl)carbodiimide hydrochloride; g.p, guinea pig; GPCRs, G-protein-coupled receptors; HATU, hexafluorophosphate azabenzotriazole tetramethyluronium; h, hour; HRMS, high-resolution mass spectra; *i.p.*, intraperitoneal; NCS, *N*-chlorosuccinimide; NBS, *N*-bromosuccinimide; QSAR, quantitative structure–activity relationship; Pfp-OH, pentafluorophenol; S1R, sigma 1 receptor; S2R, sigma 2 receptor; SARs, structure–activity relationships; SD, Sprague Dawley; THF, tetrahydrofuran

REFERENCES

- (1) Martin, W. R.; Eades, C. G.; Thompson, J. A.; Huppler, R. E.; Gilbert, P. E. The effects of morphine- and nalorphine- like drugs in the nondependent and morphine-dependent chronic spinal dog. *J. Pharmacol. Exp. Ther.* **1976**, *197*, 517–532.
- (2) Khazan, N.; Young, G. A.; El-Fakany, E. E.; Hong, O.; Calligaro, D. Sigma receptors mediated the psychotomimetic effects of *N*-allylnormetazocine (SKF-10,047), but not its opioid agonistic-antagonistic properties. *Neuropharmacology* **1984**, *23*, 983–987.
- (3) Hanner, M.; Moebius, F. F.; Flandorfer, A.; Knaus, H. G.; Striessnig, J.; Kempner, E.; Glossmann, H. Purification, molecular cloning, and expression of the mammalian sigma1-binding site. *Proc. Natl. Acad. Sci. U.S.A.* **1996**, *93*, 8072–8077.
- (4) Seth, P.; Fei, Y. J.; Li, H. W.; Huang, W.; Leibach, F. H.; Ganapathy, V. Cloning and functional characterization of a sigma receptor from rat brain. *J. Neurochem.* **1998**, *70*, 922–931.
- (5) Pan, Y. X.; Mei, J.; Xu, J.; Wan, B. L.; Zuckerman, A.; Pasternak, G. W. Cloning and characterization of a mouse sigma receptor. *J. Neurochem.* **1998**, *70*, 2279–2285.
- (6) Harrison, O. J.; Brasch, J.; Lasso, G.; Katsamba, P. S.; Ahlsen, G.; Honig, B.; Shapiro, L. Structural basis of adhesive binding by

desmocolins and desmogleins. *Proc. Natl. Acad. Sci. U.S.A.* **2016**, *113*, 7160–7165.

(7) Hayashi, T.; Su, T.-P. Sigma-1 receptor chaperones at the ER-mitochondrion interface regulate Ca(2+) signaling and cell survival. *Cell* **2007**, *131*, 596–610.

(8) Alonso, G.; Phan, V.-L.; Guillemain, I.; Saunier, M.; Legrand, A.; Anoa, M.; Maurice, T. Immunocytochemical localization of the sigma(1) receptor in the adult rat central nervous system. *Neuroscience* **2000**, *97*, 155–170.

(9) Bangaru, M. L.; Weihrauch, D.; Tang, Q. B.; Zoga, V.; Hogan, Q.; Wu, H. E. Sigma-1 receptor expression in sensory neurons and the effect of painful peripheral nerve injury. *Mol. Pain* **2013**, *9*, 1744–8069-9-47.

(10) Kulkarni, S. K.; Dhir, A. σ -1 receptors in major depression and anxiety. *Expert Rev. Neurother.* **2009**, *9*, 1021–1034.

(11) Jin, J. L.; Fang, M.; Zhao, Y. X.; Liu, X. Y. Roles of sigma-1 receptors in Alzheimer's disease. *Int. J. Clin. Exp. Med.* **2015**, *8*, 4808–4820.

(12) Nguyen, L.; Lucke-Wold, B. P.; Mookerjee, S. A.; Cavendish, J. Z.; Robson, M. J.; Scandinaro, A. L.; Matsumoto, R. R. Role of sigma-1 receptors in neurodegenerative diseases. *J. Pharmacol. Sci.* **2015**, *127*, 17–29.

(13) Tsai, S.-Y.; Hayashi, T.; Mori, T.; Su, T.-P. Sigma-1 receptor chaperones and diseases. *Cent. Nerv. Syst. Agents Med. Chem.* **2009**, *9*, 184–189.

(14) Balasuriya, D.; Stewart, A. P.; Edwardson, J. M. The σ -1 Receptor Interacts Directly with GluN1 But Not GluN2A in the GluN1/GluN2A NMDA Receptor. *J. Neurosci.* **2013**, *33*, 18219–18224.

(15) Rodríguez-Muñoz, M.; Sánchez-Blázquez, P.; Herrero-Labrador, R.; Martínez-Murillo, R.; Merlos, M.; Vela, J. M.; Garzón, J. The sigma1 receptor engages the redox-regulated HINT1 protein to bring opioid analgesia under NMDA receptor negative control. *Antioxid. Redox Signaling* **2015**, *22*, 799–818.

(16) Kim, F. J.; Kovalyshyn, I.; Burgman, M.; Neilan, C.; Chien, C.-C.; Pasternak, G. W. Sigma 1 receptor modulation of G-protein-coupled receptor signaling: potentiation of opioid transduction independent from receptor binding. *Mol. Pharmacol.* **2010**, *77*, 695–703.

(17) Zhang, H.; Cuevas, J. Sigma receptors inhibit high-voltage-activated calcium channels in rat sympathetic and parasympathetic neurons. *J. Neurophysiol.* **2002**, *87*, 2867–2879.

(18) Cendán, C. M.; Pujalte, J. M.; Portillo-Salido, E.; Montoliu, L.; Baeyens, J. M. Formalin-induced pain is reduced in sigma(1) receptor knockout mice. *Eur. J. Pharmacol.* **2005**, *511*, 73–74.

(19) Entrena, J. M.; Cobos, E. J.; Nieto, F. R.; Cendán, C. M.; Gris, G.; Del Pozo, E.; Zamanillo, D.; Baeyens, J. M. Sigma-1 receptors are essential for capsaicin-induced mechanical hypersensitivity: studies with selective sigma-1 ligands and sigma-1 knockout mice. *Pain* **2009**, *143*, 252–261.

(20) Nieto, F. R.; Cendán, C. M.; Sánchez-Fernández, C.; Cobos, E. J.; Entrena, J. M.; Tejada, M. A.; Zamanillo, D.; Vela, J. M.; Baeyens, J. M. Role of sigma-1 receptors in paclitaxel-induced neuropathic pain in mice. *J. Pain* **2012**, *13*, 1107–1121.

(21) Nieto, F. R.; Cendan, C. M.; Canizares, F. J.; Cubero, M. A.; Vela, J. M.; Fernandez-Segura, E.; Baeyens, J. M. Genetic inactivation and pharmacological blockade of sigma-1 receptors prevent paclitaxel-induced sensory-nerve mitochondrial abnormalities and neuropathic pain in mice. *Mol. Pain* **2014**, *10*, 1744-8069-10-11.

(22) Sánchez-Fernández, C.; Montilla-García, Á.; González-Cano, R.; Nieto, F. R.; Romero, L.; Artacho-Cordón, A.; Montes, R.; Fernández-Pastor, B.; Merlos, M.; Baeyens, J. M.; Entrena, J. M.; Cobos, E. J. Modulation of Peripheral μ -Opioid Analgesia by σ 1 Receptors. *J. Pharmacol. Exp. Ther.* **2014**, *348*, 32–45.

(23) Sánchez-Fernández, C.; Nieto, F. R.; González-Cano, R.; Artacho-Cordón, A.; Romero, L.; Montilla-García, Á.; Zamanillo, D.; Baeyens, J. M.; Entrena, J. M.; Cobos, E. J. Potentiation of morphine-induced mechanical antinociception by σ 1 receptor inhibition: Role of peripheral σ 1 receptors. *Neuropharmacology* **2013**, *70*, 348–358.

(24) Vidal-Torres, A.; de la Puente, B.; Rocasbalbas, M.; Touriño, C.; Andreea Bura, S.; Fernández-Pastor, B.; Romero, L.; Codony, X.; Zamanillo, D.; Buschmann, H.; Merlos, M.; Manuel Baeyens, J.; Maldonado, R.; Vela, J. M. Sigma-1 receptor antagonism as opioid adjuvant strategy: enhancement of opioid antinociception without increasing adverse effects. *Eur. J. Pharmacol.* **2013**, *711*, 63–72.

(25) Thomas, J. D.; Longen, C. G.; Oyer, H. M.; Chen, N.; Maher, C. M.; Salvino, J. M.; Kania, B.; Anderson, K. N.; Ostrander, W. F.; Knudsen, K. E.; Kim, F. J. Sigma1 targeting to suppress aberrant androgen receptor signaling in prostate cancer. *Cancer Res.* **2017**, *77*, 2439–2452.

(26) Maher, C. M.; Thomas, J. D.; Haas, D. A.; Longen, C. G.; Oyer, H. M.; Tong, J. Y.; Kim, F. J. Small-molecule sigma1 modulator induces autophagic degradation of PD-L1. *Mol. Cancer Res.* **2018**, *16*, 243–255.

(27) Gordon, D. E.; Jang, G. M.; Bouhaddou, M.; Xu, J.; Obernier, K.; White, K. M.; O'Meara, M. J.; Rezell, V. V.; Guo, J. Z.; Swaney, D. L.; Tummino, T. A.; Huttenhain, R.; Kaake, R. M.; Richards, A. L.; Tutuncuoglu, B.; Foussard, H.; Batra, J.; Haas, K.; Modak, M.; Kim, M.; Haas, P.; Polacco, B. J.; Braberg, H.; Fabius, J. M.; Eckhardt, M.; Souchery, M.; Bennett, M. J.; Cakir, M.; McGregor, M. J.; Li, Q.; Meyer, B.; Roesch, F.; Vallet, T.; Mac Kain, A.; Miorin, L.; Moreno, E.; Naing, Z. Z. C.; Zhou, Y.; Peng, S.; Shi, Y.; Zhang, Z.; Shen, W.; Kirby, I. T.; Melnyk, J. E.; Chorbha, J. S.; Lou, K.; Dai, S. A.; Barrio-Hernandez, I.; Memon, D.; Hernandez-Armenta, C.; Lyu, J.; Mathy, C. J. P.; Perica, T.; Pilla, K. B.; Ganesan, S. J.; Saltzberg, D. J.; Rakesh, R.; Liu, X.; Rosenthal, S. B.; Calviello, L.; Venkataramanan, S.; Liboy-Lugo, J.; Lin, Y.; Huang, X.-P.; Liu, Y.; Wankowicz, S. A.; Bohn, M.; Safari, M.; Ugur, F. S.; Koh, C.; Savar, N. S.; Tran, Q. D.; Shengjuler, D.; Fletcher, S. J.; O'Neal, M. C.; Cai, Y.; Chang, J. C. J.; Broadhurst, D. J.; Klippsten, S.; Sharp, P. P.; Wenzell, N. A.; Kuzuoglu-Ozturk, D.; Wang, H.-Y.; Trenker, R.; Young, J. M.; Caverio, D. A.; Hiatt, J.; Roth, T. L.; Rathore, U.; Subramanian, A.; Noack, J.; Hubert, M.; Stroud, R. M.; Frankel, A. D.; Rosenberg, O. S.; Verba, K. A.; Agard, D. A.; Ott, M.; Emerman, M.; Jura, N.; von Zastrow, M.; Verdin, E.; Ashworth, A.; Schwartz, O.; d'Enfert, C.; Mukherjee, S.; Jacobson, M.; Malik, H. S.; Fujimori, D. G.; Ideker, T.; Craik, C. S.; Floor, S. N.; Fraser, J. S.; Gross, J. D.; Sali, A.; Roth, B. L.; Ruggiero, D.; Taunton, J.; Kortemme, T.; Beltrao, P.; Vignuzzi, M.; García-Sastre, A.; Shokat, K. M.; Shoichet, B. K.; Krogan, N. J. A SARS-CoV-2 protein interaction map reveals targets for drug repurposing. *Nature* **2020**, *583*, 459–468.

(28) Cebrecos, J.; Galvez, R.; Albesa, N.; MunozBlanco, J.; Aguilar, J.; Rojals, V. M.; Casals, S.; Sust, M.; Vaqué, A.; Morte, A.; Gascón, N.; PlataSalamán, C. In E52862, a First in Class Sigma 1 Receptor Antagonist. *Chronic PostSurgical Neuropathic Pain: An Exploratory Phase II Clinical Trial, 16th World Congress on Pain, Yokohama, Japan: Yokohama, Japan, 2016.*

(29) Romero, L.; Zamanillo, D.; Nadal, X.; Sánchez-Arroyos, R.; Rivera-Arconada, I.; Dordal, A.; Montero, A.; Muro, A.; Bura, A.; Segalés, C.; Laloya, M.; Hernández, E.; Portillo-Salido, E.; Escriche, M.; Codony, X.; Encina, G.; Burguenio, J.; Merlos, M.; Baeyens, J.; Giraldo, J.; López-García, J.; Maldonado, R.; Plata-Salamán, C.; Vela, J. Pharmacological properties of S1RA, a new sigma-1 receptor antagonist that inhibits neuropathic pain and activity-induced spinal sensitization. *Br. J. Pharmacol.* **2012**, *166*, 2289–2306.

(30) Peng, Y.; Dong, H.; Welsh, W. J. Comprehensive 3D-QSAR model predicts binding affinity of structurally diverse sigma 1 receptor ligands. *J. Chem. Inf. Model.* **2019**, *59*, 486–497.

(31) Schmidt, H. R.; Zheng, S.; Gurpinar, E.; Koehl, A.; Manglik, A.; Kruse, A. C. Crystal structure of the human σ 1 receptor. *Nature* **2016**, *532*, 527.

(32) Jones, G.; Willett, P.; Glen, R. C.; Leach, A. R.; Taylor, R. Development and validation of a genetic algorithm for flexible docking. *J. Mol. Biol.* **1997**, *267*, 727–748.

(33) Schmidt, H. R.; Betz, R. M.; Dror, R. O.; Kruse, A. C. Structural basis for sigma1 receptor ligand recognition. *Nat. Struct. Mol. Biol.* **2018**, *25*, 981–987.

(34) Greenfield, D. A.; Schmidt, H. R.; Skiba, M. A.; Mandler, M. D.; Anderson, J. R.; Sliz, P.; Kruse, A. C. Virtual screening for ligand

discovery at the sigma1 receptor. *ACS Med. Chem. Lett.* **2020**, *11*, 1555–1561.

(35) Peng, Y.; Zhang, Q.; Arora, S.; Keenan, S. M.; Kortagere, S.; Wannemacher, K. M.; Howells, R. D.; Welsh, W. J. Novel delta opioid receptor agonists exhibit differential stimulation of signaling pathways. *Bioorg. Med. Chem.* **2009**, *17*, 6442–6450.

(36) Lipinski, C. A.; Lombardo, F.; Dominy, B. W.; Feeney, P. J. Experimental and computational approaches to estimate solubility and permeability in drug discovery and development settings. *Adv. Drug Deliv. Rev.* **2001**, *46*, 3–26.

(37) Baell, J. B.; Holloway, G. A. New substructure filters for removal of pan assay interference compounds (PAINS) from screening libraries and for their exclusion in bioassays. *J. Med. Chem.* **2010**, *53*, 2719–2740.

(38) Bowen, W. D.; De Costa, B. R.; Hellewell, S. B.; Walker, J. M.; Rice, K. C. [3H]-(+)-Pentazocine: A potent and highly selective benzomorphan-based probe for sigma-1 receptors. *Mol. Neuropharmacol.* **1993**, *3*, 117.

(39) Ganapathy, M. E.; Prasad, P. D.; Huang, W.; Seth, P.; Leibach, F. H.; Ganapathy, V. Molecular and ligand-binding characterization of the sigma-receptor in the Jurkat human T lymphocyte cell line. *J. Pharmacol. Exp. Ther.* **1999**, *289*, 251–260.

(40) Cao, X.; Chen, Y.; Zhang, Y.; Lan, Y.; Zhang, J.; Xu, X.; Qiu, Y.; Zhao, S.; Liu, X.; Liu, B.-F.; Zhang, G. Synthesis and biological evaluation of novel sigma1 receptor ligands for treating neuropathic pain: 6-hydroxypyridazinones. *J. Med. Chem.* **2016**, *59*, 2942–2961.

(41) Sun, H.; Shi, M.; Zhang, W.; Zheng, Y.-M.; Xu, Y.-Z.; Shi, J.-J.; Liu, T.; Gunosewoyo, H.; Pang, T.; Gao, Z.-B.; Yang, F.; Tang, J.; Yu, L.-F. Development of novel alkoxyisoxazoles as sigma-1 receptor antagonists with antinociceptive efficacy. *J. Med. Chem.* **2016**, *59*, 6329–6343.

(42) Cobos, E. J.; Baeyens, J. M.; Del Pozo, E. Phenytoin differentially modulates the affinity of agonist and antagonist ligands for sigma 1 receptors of guinea pig brain. *Synapse* **2005**, *55*, 192–195.

(43) Bowes, J.; Brown, A. J.; Hamon, J.; Jarolimek, W.; Sridhar, A.; Waldron, G.; Whitebread, S. Reducing safety-related drug attrition: the use of in vitro pharmacological profiling. *Nat. Rev. Drug Discov.* **2012**, *11*, 909–922.

(44) Tjølsen, A.; Berge, O. G.; Hunskaar, S.; Rosland, J. H.; Hole, K. The formalin test: an evaluation of the method. *Pain* **1992**, *51*, 5–17.

(45) Mogil, J. S. Animal models of pain: progress and challenges. *Nat. Rev. Neurosci.* **2009**, *10*, 283–294.

(46) Polomano, R. C.; Mannes, A. J.; Clark, U. S.; Bennett, G. J. A painful peripheral neuropathy in the rat produced by the chemotherapeutic drug, paclitaxel. *Pain* **2001**, *94*, 293–304.

(47) Hao, J.-X.; Xu, X.-J.; Urban, L.; Wiesenfeld-Hallin, Z. Repeated administration of systemic gabapentin alleviates allodynia-like behaviors in spinally injured rats. *Neurosci. Lett.* **2000**, *280*, 211–214.

(48) Ling, B.; Authier, N.; Balayssac, D.; Eschalier, A.; Coudore, F. Behavioral and pharmacological description of oxaliplatin-induced painful neuropathy in rat. *Pain* **2007**, *128*, 225–234.

(49) Altenbach, R. J.; Bogdan, A.; Couty, S.; De Lemos, E.; Desroy, N.; Duthion, B.; Gfesser, G. A.; Greszler, S. N.; Housseman, C. G.; Koenig, J. R.; Kym, P. R.; Liu, B.; Scanio, M. J.; Searle, X.; Wang, X.; Yeung, M. C.; Zhao, G. Substituted pyrrolidines and their use in the treatment of cystic fibrosis. WO 2018065962 A1, Apr 12, 2018, 2018.

(50) Chaplan, S. R.; Bach, F. W.; Pogrel, J. W.; Chung, J. M.; Yaksh, T. L. Quantitative assessment of tactile allodynia in the rat paw. *J. Neurosci. Methods* **1994**, *53*, 55–63.